Estimation of power plant SO_2 emissions using HYSPLIT dispersion model and airborne observations with plume rise ensemble runs

Tianfeng Chai[1,2,3], Xinrong Ren[1], Fong Ngan[1,2,3], Mark Cohen[1], and Alice Crawford[1]

[1]NOAA Air Resources Laboratory (ARL), NOAA Center for Weather and Climate Prediction, 5830 University Research Court, College Park, MD 20740, USA

[2]Cooperative Institute for Satellites Earth System Studies (CISESS), University of Maryland, College Park, MD 20740, USA

[3]Department of Atmospheric and Oceanic Science, University of Maryland, College Park, MD 20740, USA

Correspondence: Tianfeng Chai (Tianfeng.Chai@noaa.gov)

Abstract. The SO_2 ~~mixing ratio measurements were made by a research aircraft close to~~ emission rates from three power plants in North Carolina are estimated using the HYSPLIT Lagrangian dispersion model and the aircraft measurements made on March 26, 2019. ~~An~~ To quantify the underlying modeling uncertainties in the plume rise calculation, an ensemble of dispersion simulations ~~with HYSPLIT model v5.2.0~~ are carried out using a total of 15 heat release parameters~~ranging from 10 MW to~~

5   ~~150 MW for the Briggs plume rise calculation to quantify the underlying modeling uncertainties.~~. For each heat release~~value, a total of 72 independent HYSPLIT Lagrangian model runs with unit hourly emissions from the three point sources are made to form~~, the SO_2 emissions rates are estimated using a transfer coefficient matrix (TCM) ~~with the airborne observations. The TCMs can be decoupled into six segments where the observations of each segment are only influenced by a single power plant in its morning or afternoon operation. Prior to estimating the power plant emissions, the simulation performance is first~~

10   ~~evaluated with the correlation coefficients between the observations and the model prediction with constant unit-emission in its morning or afternoon operations~~approach and compared with the Continuous Emissions Monitoring Systems (CEMS) data. An "optimal" member is first selected based on the correlation coefficient calculated for each of the six segments that delineate the plumes from the three power plants during the morning and afternoon flights. The segment influenced by the afternoon operations of Belews Creek power plant has negative correlation coefficients for all the plume rise options and is

15   first excluded from the emission estimate ~~when the "optimal" member is selected based on the correlation coefficient. For the other segments, the plume rise runs with the highest correlation coefficients are selected for the emission estimates using the HYSPLIT inverse modeling system. In the TCM-based inverse modeling, the emission estimates are obtained by minimizing a cost function which measures the difference between logarithmic predicted and observed mixing ratios but also takes model uncertainties into account. A cost function normalization scheme is adopted to avoid spurious emission solutions when using

20   logarithmic concentration differences following Chai et al. (2018). The source estimation results of the three power plants with the morning and afternoon flight segments are compared with the Continuous Emissions Monitoring Systems (CEMS) data.~~ here. Overestimations are found for all the segments before considering the background SO_2 mixing ratios. Both constant background mixing ratios and several segment-specific background values are tested in the HYSPLIT inverse modeling. The estimation results by assuming the 25th percentile observed SO_2 mixing ~~ratio~~ ratios inside each of the five segments agree well

25   with the CEMS data, with relative errors as 18%, -12%, 3%, 93.5%, and -4%. After emission estimations are performed for all

the plume rise runs, least root mean square errors (RMSEs) between the predicted and observed mixing ratios are calculated to select a different set of "optimal" plume rise runs which have the least RMSEs. Identical plume rise runs are chosen as the "optimal" members for Roxboro and Belews Creek morning segments, but different members for the other segments yield smaller RMSEs than the previous correlation-based "optimal" members. It is also no longer necessary to exclude the Belews Creek afternoon segment that has negative correlation between predictions and observations. The RMSE-based "optimal" runs result in a much better agreement with the CEMS data for the previous severely overestimated segment and do not ~~deterioirate~~ deteriorate much for the other segments, with relative errors as 18%, -18%, 3%, -9%, and 27% for the five segments, and 2% for Belews Creek afternoon segment. ~~While~~ In addition, the RMSE-based "optimal" ~~plume rise runs appear to agree better with the observations~~ heat emissions appear to be more reasonable than the correlation-based ~~"optimal" runs~~ values when they are ~~different, significant differences exist in the area where observations are missing.~~ are compared with the CEMS (continuous emissions monitoring systems) data as well as those obtained through the simple mass balance approach. Without considering the background SO_2 mixing ratios, the power plant emissions For the Belews Creek afternoon segment, a new method is proposed to avoid direct point-to-point comparison between the model simulation results and the observations. Instead, an integrated flux density at the altitude where the maximum mixing ratio was observed is calculated for both model predictions with unit emissions and observations. The SO_2 emissions are found to be within a factor of two with respect to the CEMS estimates. A suite of air pollutant measurements were made by the University of Maryland Cessna 402B research aircraft close to three power plants in North Carolina on March 26, 2019. i A simple mass balance approach is also applied to a total of 26 transects obtained from the morning and afternoon flights. In addition, several additional ways to estimate the emissions by directly comparing the HYSPLIT dispersion results and the aircraft observations are attempted as well. The uncertainties associated with the various emission estimation methods will be discussed. significantly different for CPI Roxboro power plant.

1 Introduction

Both Eulerian and Lagrangian atmospheric transport models have been widely used to provide forecasts or analyses of atmospheric components for a wide range of purposes varying from emergency responding to climate change predictions. However, in many applications, such as volcanic eruptions, wildfire events, accidental radionuclide releases from nuclear power plants, and climate change predictions, emissions are the most critical model input parameters but are mostly unknown and difficult to quantify. Even when emission inventories are made available through bottom-up approaches, some of the emissions are often associated with large uncertainties and systematic biases due to outdated databases, inaccurate emission factors, and invalid assumptions regarding operations, processes, and/or activities (throughput) during the bottom-up emission estimation. Therefore, various inverse modeling methods using so-called top-down approaches have been developed in order to estimate the emissions by combining the direct observations and the accumulated knowledge already built into the atmospheric transport models. Lagrangian particle dispersion models are particularly suited to the applications related to point source emission estimations because they effectively avoid calculation outside air pollutant plumes and do not have numerical diffusion problems

suffered by most Eulerian models. Many source term estimation applications have been developed using various dispersion

60   models and inverse modeling schemes (e.g., Stohl et al., 2012; Winiarek et al., 2012; Saunier et al., 2013; Winiarek et al., 2014; Chai et al., 2015; Bieringer et al., 2017; Hutchinson et al., 2017; Chai et al., 2018; Kim et al., 2020).

The National Oceanic and Atmospheric Administration (NOAA) Air Resources Laboratory's (ARL) HYSPLIT Lagrangian model is one of the most extensively used atmospheric transport models to simulate the atmospheric transport, dispersion, and deposition of pollutants and hazardous materials (Draxler and Hess, 1997; Stein et al., 2015). A HYSPLIT inverse system

65   based on 4D-Var data assimilation and a transfer coefficient matrix (TCM) was developed and applied to estimate cesium-137 source from the Fukushima nuclear accident using global air concentration measurements (Chai et al., 2015). The system was further developed to estimate the effective volcanic ash release rates as a function of time and height by assimilating satellite mass loadings and ash cloud top heights (Chai et al., 2017). More recently, a HYSPLIT-based Emissions Inverse Modeling System (HEIMS) was developed to estimate wildfire emissions from the transport and dispersion of smoke plumes captured

70   by geostationary satellite aerosol optical depth observations (Kim et al., 2020). In another HYSPLIT inverse system study with the Cross Appalachian Tracer Experiment (CAPTEX) data collected from six controlled releases, Chai et al. (2018) found that adding model uncertainty terms was able to improve source estimate results.

The source term estimation problem proves to be challenging because of the chaotic nature of the atmospheric flow. In addition, the observations from routine monitoring networks are typically sparse and often do not provide enough information

75   to determine emission sources. Many field campaign studies have been carried out with airborne measurements by research aircraft in order to estimate certain air pollutant and greenhouse gas emission sources. Both traditional mass balance methods ~~(e.g., Mays et al., 2009; Cambaliza et al., 2014; Ren et al., 2018)~~(e.g., Mays et al., 2009; Cambaliza et al., 2014; Liggio et al., 2016; Ren e , and various inverse modeling methods which take advantages of atmospheric transport models (e.g., Karion et al., 2019; Angevine et al., 2020; Pitt et al., 2022; Lopez-Coto et al., 2022) have been applied to quantify different emissions. While many

80   inverse modeling applications have been carried out and compared with the bottom-up emission inventories, large uncertainties are still associated with the top-down estimations. Karion et al. (2019) showed an intercomparison study using both inventory scaling method and Bayesian inversion with several dispersion models and meteorological inputs for emission estimation with flight observations. They found significant variabilities (up to a factor of 3) between different models and between different days and indicated that further work was needed to evaluate and improve vertical mixing in the tracer dispersion models.

85   To better evaluate the top-down estimates of emissions, Angevine et al. (2020) studied a power plant with Continuous Emissions Monitoring Systems (CEMS) data as the known emissions. They used a model-assisted mass balance method and examined the estimate uncertainties with an ensemble of HYSPLIT runs with different meteorological inputs and concluded with reasonably large (30%–40%) uncertainties for the top-down estimates of emissions. However, a constant heat release of 85 MW as the main plume-rise parameter used in the Briggs formulation was specified for all the simulations.

90   This could have caused an underestimation of the uncertainties. Gordon et al. (2018) and Akingunola et al. (2018) found that the Briggs plume rise algorithm (Briggs, 1984) significantly underestimated plume rise, in contrast to the majority of past plume rise measurement studies. A recent study by Kim et al. (2023) to estimate power plant SO_2 emission rates with aircraft

measurements also highlighted the large uncertainties caused by the plume rise calculation when using a Gaussian footprint approach.

95   Fathi et al. (2021) investigated the impact of storage-and-release due to meteorological variability on mass-balance emission rate retrieval accuracy using virtual aircraft sampling of a regional chemical transport model output. The storage-and-release events contributed to the mass-balance emission estimate errors ranging from -25% to 24% in their tests. They recommended repeat flights around the given facility and/or time-consecutive upwind and downwind vertical profiling during the sampling period. However, inverse modeling methods using a dispersion model without assuming constant meteorological fields is

100   expected to perform better than the mass balance method.

    In this study, the HYSPLIT inverse modeling system is tested with flight observations collected in 2019 by the University of Maryland Cessna 402B research aircraft to estimate SO_2 point source emissions from three power plants in North Carolina, USA. An ensemble of model runs with a range of emission heat release parameters are used to quantify the forward model simulation uncertainties due to the plume rise calculation. The paper is organized as follows. Section 2 describes the flight

105   observations as well as the HYSPLIT model configuration, and the source term inversion method. Section 3 presents emission inversion results and a summary is given in Section 4.

2   Methods

2.1   Observations

    A suite of airborne measurements were collected using an instrumented small research aircraft, University of Maryland Cessna

110   402B on March 26, 2019. A morning flight started from 13:45 to 17:38 UTC and an afternoon flight lasted from 19:31 to 23:33 UTC. The flight tracks and the locations of the power plants are shown in Fig 1. The flights were intended to sample downwind plumes originated from three coal-fired power plants in North Carolina, Roxboro (36.4833°N 78.0731°W), CPI Roxboro (36.4350°N 78.9619°W), and Belews Creek (36.2811°N 80.0603°W). Note that another power plant, Mayo (36.5278°N 78.8917°W), is also in the region, but did not operate on the day. Measurement of SO_2 mixing ratios was made with a Thermo

115   Environment Model 43S pulsed fluorescence analyzer. Calibration of the SO_2 analyzer was conducted before and after the field study with an SO_2 standard that is traceable to National Institute of Standards and Technology (NIST) reference standards. Additional measurements were also made, including aircraft locations, wind speed, wind direction, temperature, pressure, relative humidity, and mixing ratios of several other gas species, as well as some aerosol optical properties. More details related to the aircraft instruments and measurements can be found in Ren et al. (2018).

120   To better compare the HYSPLIT model results with the observations, the original 1-sec data are averaged inside each four-dimensional (4-D) HYSPLIT sampling grid box, i.e., 0.01° longitude by 0.008° latitude, 100 m in altitude, and 1 minute in time in this application. It should be noted that the aircraft typically travels several three-dimensional (3-D) grid boxes within a minute. The original 1-sec data inside each 3-D grid box are averaged separately so that multiple 1-min records would result from such a 4-D averaging. For brevity, the 4-D averaged data are still referred as 1-min data hereafter.
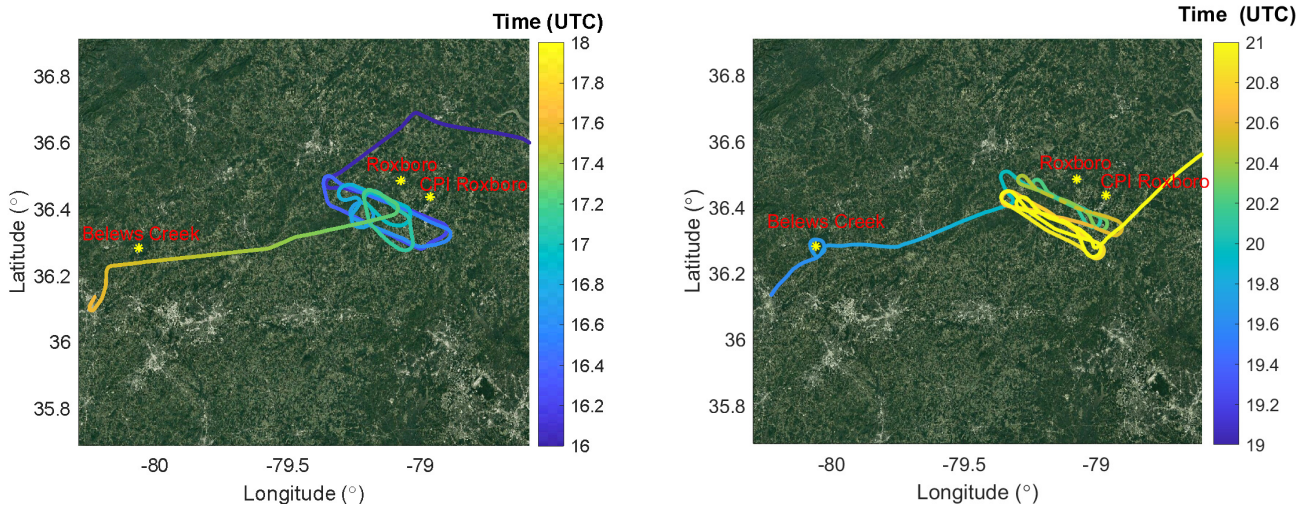
Figure 1. Flight tracks of the morning (left) and afternoon (right) flights on March 26, 2019 on top of the ©Google Maps satellite image (retrieved in February 2023). Color represents the aircraft travel time of the day (UTC). The locations of Belews Creek, Roxboro, and CPI Roxboro power plants are also shown.

2.2 HYSPLIT model

In this study, SO_2 plumes originated from the power plants are modeled using the HYSPLIT model (Version 5.2.0) in its particle mode in which three-dimensional (3D) Lagrangian particles released from the source location passively follow the wind field~~(Draxler and Hess, 1997, 1998; Stein et al., 2015).~~ Random velocity components based on the meteorological data are added to the mean advection velocities to simulate the dispersion process. The details of the model can be found in Draxler and Hess (1997, 1998) and Stein et al. (2015). Green et al. (2019) found that the SO_2 oxidation rates during the day from power plants were 0.22–0.71%/hr, using 13 flights from 6 February to 15 March 2015 over the eastern United States. The measurements were made during a clear-sky day on March 26, 2019 and the travel time of the measured air parcels from the stacks are less than three hours. So it is reasonable to treat SO_2 as a passive tracer and ignore its oxidation. A particle release rate of 20,000 per hour is used for all calculations. The meteorological data used to drive HYSPLIT are from the Weather Research and Forecasting (WRF; version 4.0.1) model (Powers et al., 2017)~~at 3 km horizontal grid spacing (D03 in Fig. 2) and 5-minute temporal frequency.~~ The WRF model was configured for three-nested domains with horizontal grid spacing of 27 km (D01), 9 km (D02), and 3 km (Figure 2). A total of 33 vertical layers were defined with a higher resolution near the surface and 100 hPa for model top. There were 20 layers below 850 hPa with the first mid-layer height of the model at around 8 m. The simulations for the D01 were initialized by using the North American Regional Reanalysis (Mesinger et al., 2006) with 32-km grid spacing and available every 3 h. Then, the WRF results from the coarser domains provided the initial and boundary conditions for the inner domains. The daily WRF runs had a 30-hr duration including 6-hr a spin-up period (i.e., starting at 18 UTC on the previous day). The physics options for the WRF simulations were - the rapid radiative

transfer model for radiation parameterization (Iacono et al., 2008), WSM6 for microphysics i(Lim and Hong, 2010), the Grell 3D Ensemble for the sub-grid cloud scheme (Grell and Devenyi, 2002), Noah land-surface model (Chen and Dudhia, 2001),

145 and Mellor-Yamada-Nakanishi-Niino 2.5 level TKE scheme for the planetary boundary layer (PBL) parameterization and its corresponding surface layer scheme (Nakanishi and Niino, 2006). In the WRF simulations, 3D grid nudging of winds is applied in the free troposphere and within the ~~planetary boundary layer (PBL). Fig.~~PBL. Figure 3 shows that the WRF wind speed data mostly agree well with the aircraft observations. However, at the beginning of the afternoon flight the 1-min observations show large variations in wind direction that the 5-min WRF data cannot represent. ~~Note that the WRF simulations of the two~~

150 ~~outer domains (D01 and D02 in Fig. 2) are generated to provide boundary conditions for the most inner domain D03.~~ The WRF turbulent kinetic energy (TKE) data are used to calculate the turbulent velocity variances. The ratios of the vertical to the horizontal turbulence for daytime and nighttime are set as 0.18 for both daytime and nighttime. The boundary layer stability is computed from the heat and momentum fluxes from the meteorological data. The WRF mixed layer depth is directly used in the HYSPLIT model.
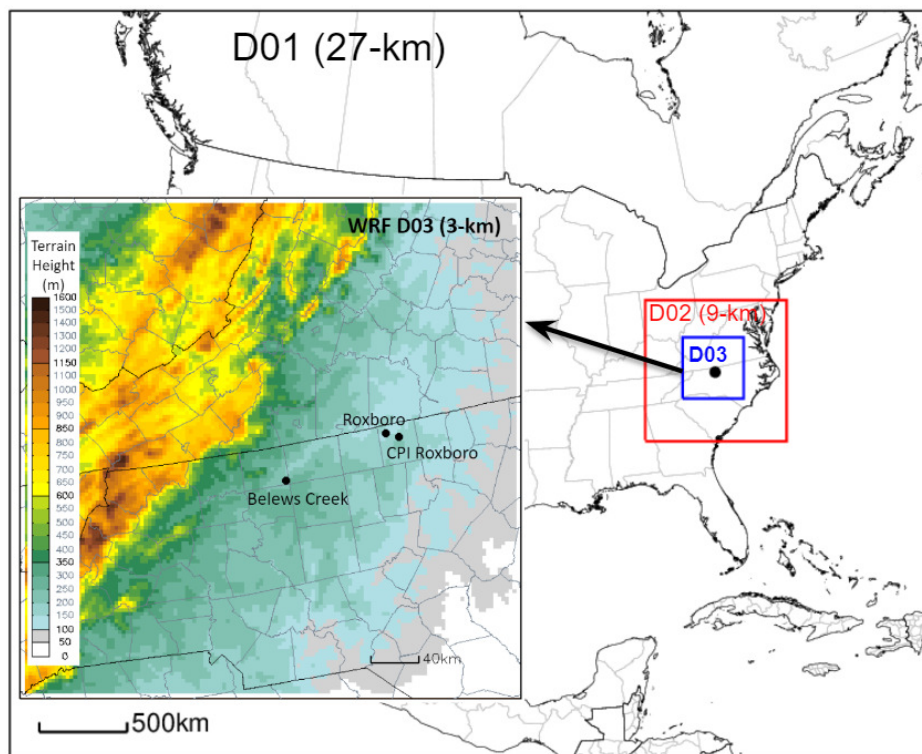
Figure 2. Three nested domains D03, D02, and D01 used in WRF simulations at 3 km, 9 km, and 27 km, respectively.

155 The dry deposition velocicy of SO_2 is calculated using the resistance method ~~by the HYSPLIT model where~~ following Wesely (1989), Chang et al. (1990), and Walmsley and Wesely (1996). Note that the canopy resistance component depends upon a number of plant physiological and ground surface characteristics which are provided to the HYSPLIT model by a land
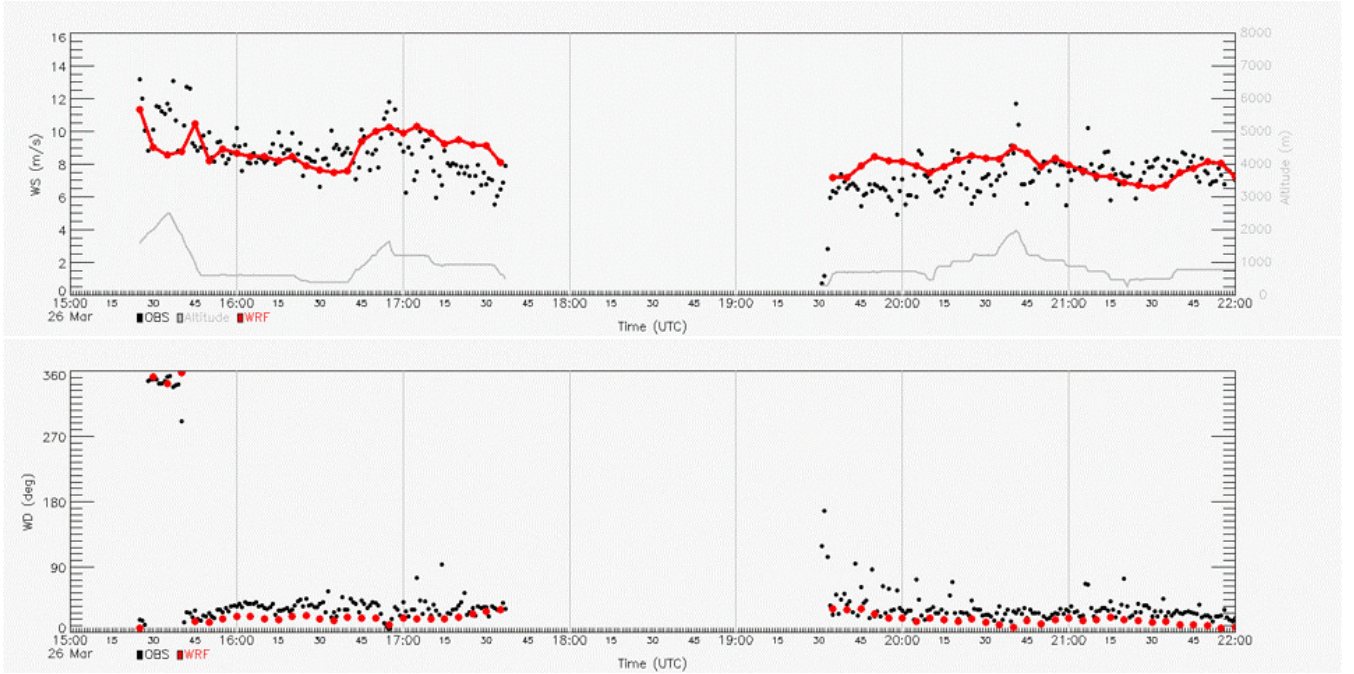
Figure 3. Wind speed (top) and wind direction (bottom) comparisons between the 1-min aircraft measurements (OBS) and 5-min WRF data along the flight. Aircraft above ground level altitudes are also shown.

use input file. The molecular weight, diffusivity ratio, and effective Henry's law constant are specified as 64 g/mol, 1.9, and 1×10^5 mol/L/atm, respectively. Actual Henry's constant of 1.24 mol/L/atm is used to define the wet removal process for

160   SO_2 as a soluble gas. The sampling grid is defined to be 0.01° longitude by 0.008° latitude, 100 m in altitude from surface to 2000 m above ground level. Mass mixing ratios are output every minute by setting the HYSPLIT parameter ICHEM = 6 to divide output mass by air density. They are later converted to volume mixing ratios by multiping by the molecular weight ratio of air to SO_2.

2.3   Plume rise

165   The plume rise calculation in HYSPLIT is based on the Briggs formula derived from dimensional analysis for buoyancy-dominated plume from power plant stacks ~~(Briggs, 1969)~~(Briggs, 1969, 1984). Equation 1 shows the formulas used in the HYSPLIT model for the final plume rise ΔH in different meteorological conditions following Arya (1999).

$$\Delta H = \begin{cases} 1.3\frac{F_b}{\bar{u}u_*^2}, & neutral, \; unstable \\ 2.6F_b^{1/3}\bar{u}^{-1/3}s^{-1/3}, & stable, \bar{u} > 0.5 \; m/s \\ 5.3F_b^{1/4}s^{-3/8}, & stable, \bar{u} \leq 0.5 \; m/s \end{cases} \tag{1}$$

where F_b is the buoyancy flux term, $\bar{u}$ is the mean wind speed, u_* is the friction velocity, and s is the static stability parameter, as defined in Equation 2.

$$s = \frac{g}{T_v} \frac{\partial \bar{\theta}_v}{\partial z} \qquad (2)$$

Here g is gravitational acceleration. T_v is the moist air virtual temperature and $\bar{\theta}_v$ is the mean virtual potential temperature. Note that the stability parameter is calculated using the surface conditions of the meteorological data in the HYSPLIT model. A recent study by Akingunola et al. (2018) suggests a layered buoyancy approach that allows stability to change with height for the Briggs plume rise calculation. However, the layered approach is not implemented in the HYSPLIT model yet. The buoyancy flux term F_b is approximated by Equation 3 (Briggs, 1969).

$$F_b = \frac{gQ_H}{\pi c_p \rho T} \approx 8.8 \times 10^{-6} [\frac{m^4/sec^3}{watts}] Q_H[watts], \qquad (3)$$

where c_p, ρ, and T are the specific heat at constant pressure, average density, and temperature of ambient air, respectively. Q_H is the heat emission from the stack. Assuming standard atmosphere, Q_H is the only user input parameter besides meteorological conditions that affects the final plume rise height ΔH. It is possible to calculate Q_H when the relevant parameters such as the flow rate and gas temperature at the stack exit are available. However, the exit gas temperature of the three stacks during the study period cannot be obtained. Note that even if Q_H can be accurately estimated, the ΔH calculation through Equation 1 is still subject to significant uncertainties due to some assumptions for simplification. In addition, when certain parameters are not readily available, it is preferable to assume them as unknown to allow better applicability for the source term estimation method. Thus we use a range of Q_H values for plume rise height calculation to form an ensemble of dispersion runs and the "optimal" plume rise runs that best matches the observations will be selected afterwards. In the detailed studies at six Tennessee Valley Authority over many years, it was found that heat emissions ranged from 20 to 100MW per stack with one to nine stacks operating (Briggs, 1969). For each stack in operation, 15 heat emission values uniformly distributed from 10MW to 150MW are tested in HYSPLIT simulations. During the study period, only one stack was operating at each of the three power plants.

2.4 Inverse modeling method

Similar to the previous HYSPLIT inverse modeling applications (e.g., Chai et al., 2015, 2017, 2018; Kim et al., 2020; Crawford et al., 2022), a transfer coefficient matrix (TCM) approach is used for the inverse modeling application. After a stack heat emission scenario is specified, 24 independent HYSPLIT Lagrangian model runs with unit hourly emissions starting from 0Z to 23Z on March 26, 2019 are made at each power plant to form a TCM using the 4-D averaged 1-min airborne SO_2 observations. A transfer coefficient at row m and column n of the TCM represents the source-receptor sensitivity of observation m with respect to the nth unit emission run from a certain source location and release hour. The unknown emissions can be solved by minimizing a cost function that integrates the differences between model predictions and observations, deviations of the final solution from the first guess (*a priori*), as well as other relevant penalty terms if needed (Daley, 1991). Following Chai et al. (2018), a cost function normalization scheme is introduced and the cost function $\mathcal{F}$ is defined as,

$$\mathcal{F} = \frac{1}{2} \sum_{i=0}^{23} \sum_{j=1}^{3} \frac{(q_{ij} - q_{ij}^b)^2}{\sigma_{ij}^2} + \frac{1}{2} \sum_{m=1}^{M} \frac{(c_m^h - c_m^o)^2}{\epsilon_m^2} \times \frac{\sum_{m=1}^{M} \frac{1}{\epsilon_m^{b\ 2}}}{\sum_{m=1}^{M} \frac{1}{\epsilon_m^2}} \tag{4}$$

where q_{ij} is the discretized source term at hour i and location j for which an independent HYSPLIT simulation has been run and recorded in a TCM. q_{ij}^b is the first guess or *a priori* estimate and σ_{ij}^2 is the corresponding error variance. We assume the uncertainties of the release at each time-location are independent of each other so that only the diagonal term of the typical *a priori* error variance σ_{ij}^2 appears in Equation 4. c^h and c^o denote HYSPLIT-predicted and measured mixing ratios, respectively. The observational errors ϵ_m are assumed to be uncorrelated. Since the term ϵ_m^2 is essentially used to weight $(c_m^h - c_m^o)^2$ terms, the uncertainties of the model predictions and the representative errors are included besides the observational uncertainties.

To consider ϵ^2 in a simplified way, it is formulated as

$$\epsilon_m^2 = (f^o \times c_m^o + a^o)^2 + (f^h \times c_m^h + a^h)^2 \tag{5}$$

As the additive term parameters a^o and a^h affect the ϵ^2 in a similar way, the representative errors caused by comparing the measurements with the predicted concentrations averaged in a grid can be included in either a^h or a^o. The multiplying factor applied to the second term is the normalization to avoid having zero source as a spurious solution when logarithmic metric is used in the cost function. ϵ_m^b is the total uncertainties when q_{ij}^b is initially used in the model predictions. The details of the normalization can be found in Chai et al. (2018).

Chai et al. (2018) shows that the logarithmic metric yields better inversion results than the original air concentration metric. In this application, the metric variable in Equation 4 is changed to $ln(c)$, i.e., replacing $(c_m^h - c_m^o)$ with $ln(c_m^h) - ln(c_m^o)$. In such a case, $\epsilon_m^{ln(c)}$ is comprised of two parts, as

$$(\epsilon_m^{ln(c)})^2 = [ln(1 + f^o + \frac{a^o}{c_m^o})]^2 + [ln(1 + f^h + \frac{a^h}{c_m^h})]^2 \tag{6}$$

Note that a constant small mixing ratio 10^{-6} ppbv is added to denominators c_m^o and c_m^h to avoid division by zero.

3 Results

3.1 Transfer coefficient matrix

As mentioned in Section 2.4, a TCM approach is used in the inverse modeling. The time varying model predictions of each independent HYSPLIT Lagrangian model run with unit hourly emission at all the receptor time and locations are recorded as the transfer coefficients (TCs). The transfer coefficients from a set of model runs can be combined to generate a transfer coefficient matrix (TCM). Figure 4 shows a TCM with 72 columns separately into three parts representing the three power plants. Each of the 24 columns for a power plant represents a HYSPLIT run with unit hourly SO_2 emission specified for a single hour on March 26, 2019. Each row indicates a 1-min 4D SO_2 observation with at least a non-zero transfer coefficient obtained from the 72 HYSPLIT runs. The stack heat emission $Q_H = 50$ MW is specified for all the 72 runs. A total of 464

out of 1503 1-min 4D SO_2 observations are affected by the three power plants during this test period, according to this set of HYSPLIT runs. Among those 464 observations, the first 234 1-min observations belong to the morning flight and the next

230   230 observations are from the afternoon flight. Most of the observations with zero transfer coefficients for all the 72 HYSPLIT runs have low SO_2 mixing ratios, which are likely due to SO_2 background caused by other minor sources than the three power plants. Note that the background SO_2 mixing ratio may vary from one location to another and from one hour to the next hour.

Figure 4 shows that the emissions before 15Z or after 21Z of the day from any of the three power plants do not contribute to the predicted SO_2 plumes along the tracks of the morning or afternoon flights. Apparently the SO_2 emitted from the power

235   plant stacks before 15Z have been transported out of the region when the aircraft measurement were made along the flight routes. Figure 1b shows that aircraft has left the domain of interest at 21Z so that SO_2 emitted after 21Z were not sampled either. For 463 of the 464 indexed observation rows in ~~Fig.~~Figure 4, the non-zero transfer coefficients only appear in one of the three parts. That is, all observations except one are only affected by a single power plant for the current set of model runs. The only exception (I_{obs} = 369) of the 1-min observations is influenced by both Roxboro and CPI Roxboro. When stack

240   heat emission $Q_H = 60$ MW or higher values is applied, the plumes from the three power plants are all separate without any overlapping. This implies a decoupled system in which the emission sources from the three different power plants can be solved separately. However, with lower heat emissions ($Q_H = 10$ MW, 20 MW, 30 MW, 40 MW) some isolated 1-min observations may be influenced by both Roxboro and CPI Roxboro. The largest number of such observations appears when $Q_H = 10$ MW is applied to all three power plants where 6 of the 479 observations with non-zero transfer coefficients are affected by both

245   Roxboro and CPI Roxboro. It is found that estimating the emissions from each power plant separately by ignoring the coupling effect or by removing such rare observations yields near identical solutions.

It is also found that the observations from the morning flights (I_{obs} = 1–234) and afternoon flights (I_{obs} = 235–464) are affected by different set of hourly emissions. That is, none of the 72 hourly emission HYSPLIT runs contribute to both the morning flights and afternoon flights. The observations of the morning flight help to constrain the hourly emissions at 15Z,

250   16Z, and 17Z from Roxboro, the hourly emissions at 16Z and 17Z from Belews Creek, and the hourly emissions at 15Z, 16Z from CPI Roxboro; while the observations of the afternoon flight help to constrain the hourly emissions at 19Z, 20Z from Roxboro, the hourly emissions at 18Z and 19Z from Belews Creek, and the hourly emissions at 19Z and 20Z from CPI Roxboro. However, some of hourly emissions will not be well-constrained. For instance, the hourly emissions at 18Z from Roxboro can only be constrained by 6 1-min SO_2 mixing ratio observations and the hourly emission at 18Z from Belews

255   Creek can only constrained by 5 observations. Figure 4 shows that each observation row has only one or two non-zero TC values. If there are two non-zero TC values for any observation row, they are in two consecutive columns which represent two HYSPLIT runs with hourly emissions at two consecutive hours. Instead of trying to estimate the emissions at the individual hours from each power plant, here we will only estimate the average emissions of the two or three consecutive hours that can be constrained by the morning or afternoon flights. With this decoupling approach, the cost function minimization becomes a

260   very simplified problem.
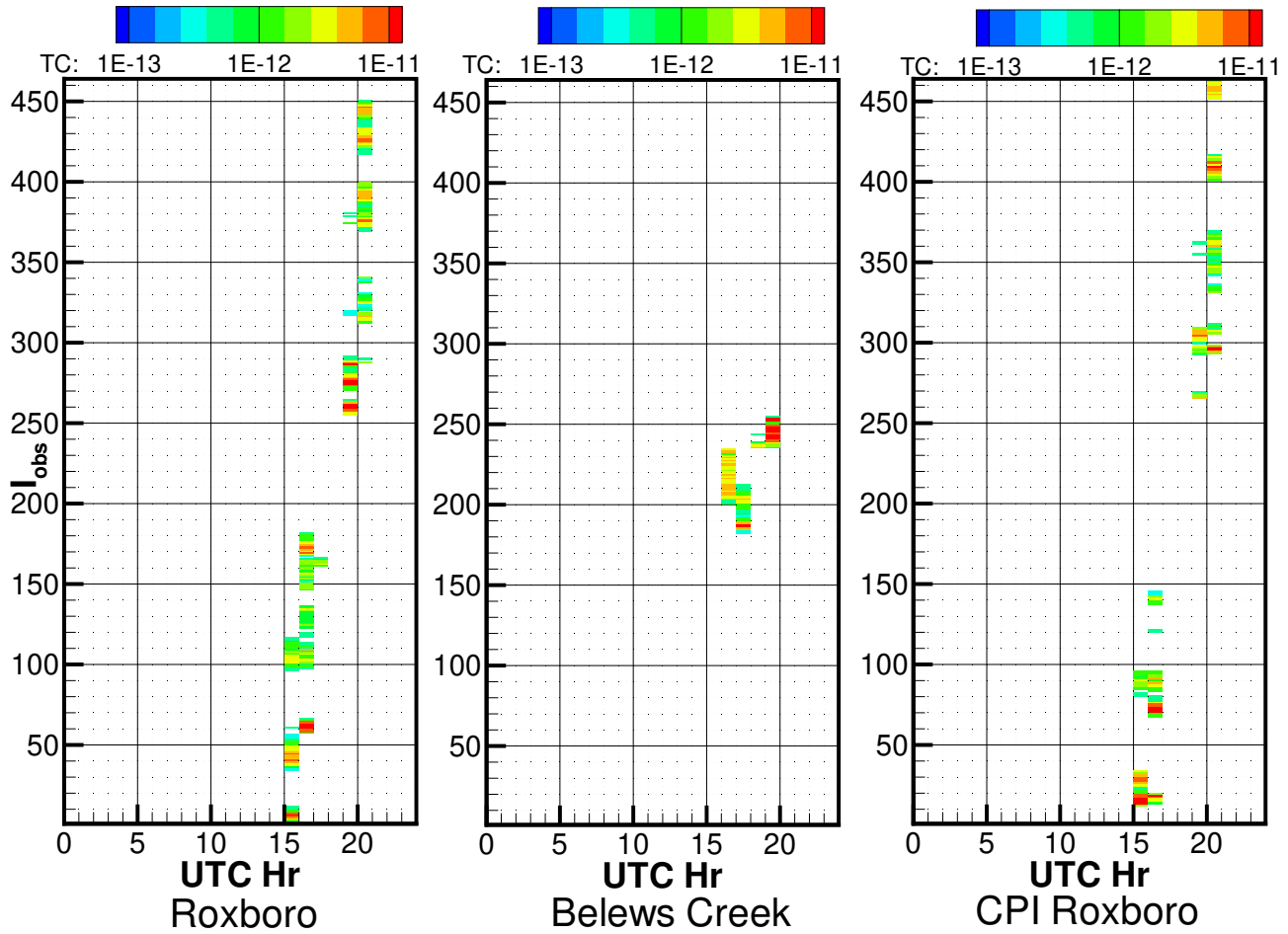
Figure 4. Transfer coefficients (TCs) calculated with unit hourly SO_2 emissions starting from 0Z to 23Z on March 26, 2019 at the three power plants with $Q_H = 50$MW. I_{obs} is the index of the 1-min 4D observations ordered by their measurement time. Observations with zero transfer coefficients for all the 72 HYSPLIT runs are excluded. The first 234 1-min observations belong to the morning flight and the next 230 observations are from the afternoon flight. TC units: ppbv/(kg/hr).

3.2 Stack heat emission

As described in Section 2.3, when other meteorological parameters are fixed, the stack heat emission Q_H becomes the single user input parameter to affect plume rise calculation with the Briggs formula being used in HYSPLIT. A total of 15 Q_H values from an expected range of 10 MW to 150 MW are tested. For each heat emission value, 24 independent HYSPLIT Lagrangian 265   model runs with unit hourly emissions starting from 0Z to 23Z on March 26, 2019 are made at each power plant, resulting in a total of 1080 model simulations. Figure 5 shows some of the plume rise results at the three different power plant locations. Note

that the plume rise is added to the stack height listed in Table 2 for the virtual release height used in the model. The plume rise mostly goes up during the day, following the PBL development. Figure 5 also shows that the WRF PBL heights appear to be underestimated when compared with the two observation-based PBL heights estimated using the vertical potential temperature profiles. Because Roxboro and CPI Roxboro are close to each other, both the PBL heights and the plume rise results with the same $Q_H = 50$ MW are quite similar. Increasing heat emission from $Q_H = 50$MW to $Q_H = 100$MW at Belews Creek results in almost doubled plume rise. Conversely, a decreased heat emission from $Q_H = 50$MW to $Q_H = 20$MW had the plume rise drastically reduced.
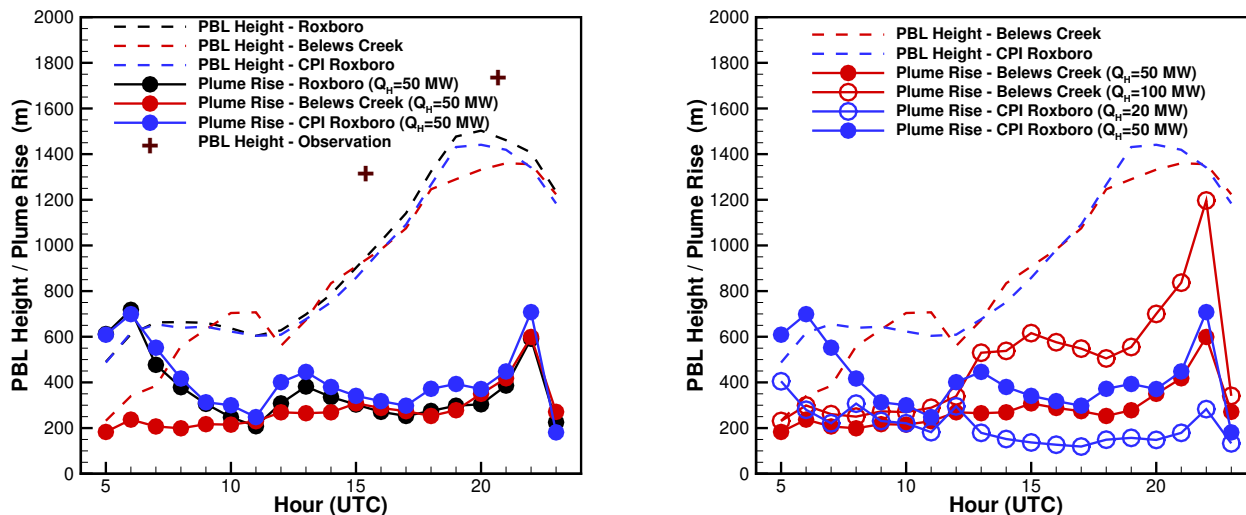
Figure 5. PBL heights and the final plume rise calculated with $Q_H = 50$ MW at three different power plant locations from 5Z to 23Z on Mar. 26, 2019 (left). Two observation-based PBL heights estimated using the vertical profiles of the potential temperature from the morning and after flight measurements are also marked. Plume rise calculated with $Q_H = 100$ MW at Belews Creek and $Q_H = 20$ MW at CPI Roxboro are compared with those calculated with $Q_H = 50$ MW. Both PBL heights and plume rise shown are above ground level (AGL) heights.

For each heat emission value applied to a power plant, the 24 HYSPLIT simulations with unit hourly emissions can be combined together to generate the SO_2 plume patterns for the particular power plant. Unless there are significant hourly emission variations the correlation coefficients (r) between the combined plume and the observations is a good metric to evelute the model performance without the need to estimate the emission magnitudes. Figures 6 shows the correlation coefficients between 1-min aircraft SO_2 observations and the unit-emission HYSPLIT simulations with different heat emission from the three power plants. When calculating model counterparts of the observations, both horizontally nearest neighbor and interpolation approaches are used. Note that the horizontal interpolation will increase the number of non-zero transfer coeffients in TCMs. For instance, the number of non-zero rows of the TCM in Fig.Figure 4 increases to 570 with horizontal interpolation from the previous 464 with nearest neighbor option. In addition, the interpolation helps to smooth the gridded predictions. Figure 6
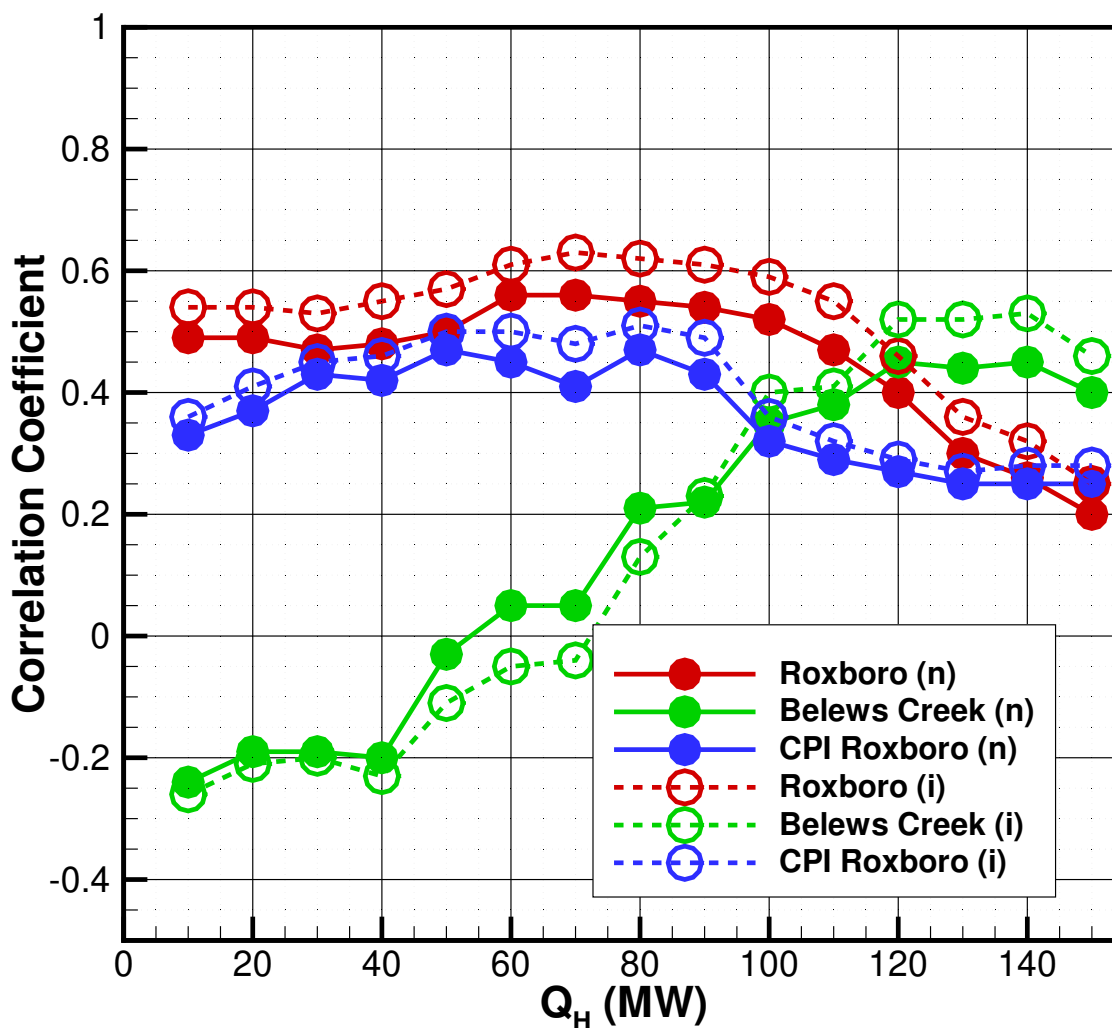
Figure 6. Correlation coefficients between 1-min SO_2 observations and the model counterparts using unit-emission HYSPLIT simulations with different heat emissions (Q_H) from the three power plants. When calculating model counterparts of the observations, both horizontally nearest neighbor (n) and interpolation (i) approaches are used.

shows that correlation coefficients typically improve by up to 0.1 using the interpolation option. All the results presented later are with horizontal interpolation when calculating model counterparts of the observations. For Roxboro plume, the HYSPLIT
285 simulation with Q_H between 60 MW and 90 MW yield fairly good correlation between the crude predictions and observations,

with r equal to or better than 0.6. The best Q_H for CPI Roxboro that generates better pattern matches with the observed SO_2 mixing ratios is probably between 40 MW and 90 MW, with r close to be 0.5. However, the simulated plume from Belews Creek only reach reasonable correlation coefficients of $r = 0.5$ when Q_H is between 120 MW and 140 MW. When Q_H is below 80 MW, low and even negative correlation coefficients appear between the predictions and observations. This will be investigated later by separating the morning and afternoon flights.

Table 1. Correlation coefficients between 1-min SO_2 observations from the morning and afternoon flights and the model counterparts using the unit-emission HYSPLIT simulations with different heat emissions from the three power plants. The highest correlation for each flight segment is highlighted with bold font.

Correlation coefficient/	Roxboro		Belews Creek		CPI Roxboro	
Heat emission (MW)	am flight	pm flight	am flight	pm flight	am flight	pm flight
10	0.61	0.46	0.45	-0.62	0.52	0.05
20	0.60	0.46	0.49	-0.69	0.60	0.06
30	0.60	0.44	0.63	-0.64	0.66	0.09
40	0.62	0.49	0.63	-0.52	0.72	0.10
50	0.60	0.55	0.73	-0.28	0.69	0.19
60	0.67	0.58	0.83	-0.22	0.72	0.20
70	**0.68**	0.58	0.86	-0.28	0.69	0.22
80	0.64	0.61	**0.87**	-0.33	0.74	0.29
90	0.60	0.62	0.83	-0.58	**0.75**	0.35
100	0.55	**0.64**	0.82	-0.62	0.64	0.34
110	0.51	0.60	0.79	*-0.68*	0.37	0.40
120	0.40	0.54	0.82	-0.67	0.20	0.41
130	0.26	0.49	0.84	-0.65	0.14	0.40
140	0.21	0.50	0.74	-0.53	0.10	**0.44**
150	0.15	0.46	0.68	-0.56	0.10	0.44

Table 1 shows the correlation coefficients between 1-min aircraft SO_2 observations from the morning and afternoon flights and the model counterparts using the unit-emission HYSPLIT simulations with different heat emission from the three power plants. For Roxboro, the HYSPLIT simulation with Q_H = 70 MW yields the best correlation coefficient $r = 0.68$ for the morning flight, but the best correlation coefficient $r = 0.64$ for the afternoon is obtained when Q_H is given as 100 MW. In fact, the power plant emissions had variations among the operation hours during the day. The HYSPLIT predictions of the morning and afternoon flight observation are contributed by the unit hourly emission runs from 15Z to 17Z and 19Z to 21Z, respectively. The CEMS SO_2 hourly emissions at Roxboro are 582, 345, and 360 kg/hr for hours 15Z, 16Z, and 17Z, respectively; 465 and 486 kg/hr for hours 19Z and 20Z, respectively. The lower average hourly emission (429 kg/hr) contributing to the morning

flight than the higher average hourly emission (476 kg/hr) contributing to the afternoon flight suggests that a higher Q_H for the afternoon flight than the morning flight since the emission of SO_2 and heat emission are expected to be proportional to each other for a particular stack. This agrees with the findings here, i.e., an higher "optimal" Q_H (100 MW) is needed for a better simulation of the afternoon flight than the "optimal" Q_H (70 MW) for the morning flight.

For Belews Creek plume, the model results with $Q_H = 80$ MW seems to capture the plume pattern recorded by the the morning flight, with a correlation coefficient $r = 0.87$ between the 1-min observations and the HYSPLIT counterparts. However, the correlation coefficients between HYSPLIT predictions and the afternoon flight observations are all negative with all the 15 Q_H values. This implies other problems rather than plume height calculation with HYSPLIT. As shown in ~~Fig.~~ Figure 3, there are large discrepancies between the WRF wind directions and the aircraft measured ones at the beginning of the afternoon flight near Belews Creek (see ~~Fig. 1~~ Figure 1). An attempted assimilation of aircraft wind measurements using the WRF observational nudging is not quite effective to correct the wind direction biases. In addition, successful predictions of the measured SO_2 require wind field measurements at the upwind locations in an earlier time period, which are not available for the current case. No "optimal" plume rise will be selected for this segment before Section 3.3.3.

The HYSPLIT simulations with $Q_H = 90$ MW and $Q_H = 140/150$ MW are found to correlate best with the CPI Roxboro SO_2 plumes measured during the morning and afternoon flights, with correlation coefficients as 0.75 and 0.44, respectively. The CEMs SO_2 hourly emissions at Roxboro CPI are 281 and 300 kg/hr for hours 15Z and 16Z, respectively; 316 and 295 kg/hr for hours 19Z and 20Z, respectively. While the fact that the optimal Q_H is higher in the afternoon corresponds well with the higher average SO_2 emission from the CPI Roxboro power plant, 306 kg/hr for 19–20Z versus 291 kg/hr for 15–16Z, the much lower correlation coefficient $r = 0.44$ for the afternoon plume indicates large prediction errors even with the "optimal" Q_H (140/150 MW).

Table 1 also hows that the model simulation generally performs better in the morning than in the afternoon. This is probably related to the fact that the wind directions in the afternoon are more variable than in the morning, as shown in Figure 3. The meteorological variability may cause storage-and-release events which make successful emission estimation more difficult to obtain, especially for the mass balance method (Fathi et al., 2021).

3.3 Inversion results

It has been shown that the current problem can be decoupled among the three different power plants. In addition, the SO_2 measurements from the power plant plumes during the morning and afternoon flights are affected by emissions of distinctive periods of two to three hours. Thus six segements are considered independently. Considering the very limited number of 1-min observations to constrain the emissions at certain hours as discussed in Section 3.1, constant emissions are assumed for each of the six segments.

When pre-processing the observations, multiple 1-second SO_2 are averaged to generate 1-min observation. The standard deviation of the multiple original 1-sec observations is calculated to represent the observational uncertainty. The parameters in Equation 5 are found using linear regression, as $f^o = 0.1$ and $a^o = 0.05$ ppbv. Chai et al. (2018) ~~shows that~~ found that the inversion results were not very sensitive to the observation uncertainty estimates. They also showed that setting the model

uncertainty parameter $f^m = 0.2$ ~~yields~~ yielded good results when compared with the known emission sources in the case study. Here the model uncertainty parameter $f^m = 0.2$ is also assumed and the additive term a^m is set as 0.05 ppbv, identical to a^o.

335   3.3.1   Zero background

Inversion estimations are first carried out without subtracting any background SO_2 mixing ratios from the observations. That is, the observations are assumed originating only from the three power plant sources. Emission estimation results of the three power plants obtained by minimizing the cost functions using the morning and afternoon flights separately are listed in Table 3 with 15 different assumed heat emissions.

340   Based on the morning flight, the estimated Roxboro SO_2 emission varies from 701.5 kg/hr with $Q_H = 10$ MW to 473.2 kg/hr with $Q_H = 150$ MW. With the "optimal" Q_H=70 MW, SO_2 emission is estimated as 551.9 kg/hr, 29% greater than the average CEMS between 15Z and 17Z. Table 2 shows the emission at 14Z and 15Z are both 582 kg/hr, while the emissions at 16Z and 17Z decrease to 345 and 360 kg/hr before going up again to 509 kg/hr at 18Z. The average emission from 19Z to 20Z estimated based on the afternoon flight with the "optimal" $Q_H = 100$ MW is 520.9 kg/hr, 9% larger than the average

345   CEMS value. Contrary to the morning flight, the estimated emissions are generally greater with increasing emission heat. The estimated emissions are 875.7 and 449.3 kg/hr with $Q_H = 150$ and 10 MW, respectively.

Using the morning flight observations, Belews Creek SO_2 emissions between 16Z and 17Z are overestimated with all 15 heat emissions. With the "optimal" $Q_H = 80$ MW, the estimated emission is 1417.3 kg/hr. Although this is 57% larger than the average CEMS emission, it is better than the estimates with other Q_H values except $Q_H = 100$ or 120 MW which yields

350   slightly lower emissions (1417.3/1406.0 kg/hr).

It is also noted that estimated Belews Creek SO_2 emissions using the afternoon flight observations are mostly within a factor of two when comparing with the average hourly CEMS emission while significant negative correlations are found between the observations and the model predictions. The worst underestimations when $Q_H = 40$–70 MW are associated with lower absolute correlations ($|r| < 0.3$). At $Q_H = 110$ MW when the most extreme anticorrelation ($r = -0.68$) occurs, the estimated

355   SO_2 emission of 697.3 kg/hr is very close to the average hourly CEMS emission of 794 kg/hr between 18Z and 19Z. The inverse correlation is caused by the plume misplacement mostly due to wind direction error. The high absolute correlation indicates that the model probably predicts the mixing ratio gradient relative well but misplaces the plume relative to actual plume. Since the model predicts higher mixing ratios when observation values are low but predicts lower mixing ratios when observation values are higher, neither lower or higher emissions would improve the agreement between the predictions and

360   observations. Thus, no significant biases arise from such cases. Nonetheless, the negative correlations between model and observations indicate model deficiencies and require special attention.

The CPI Roxboro emission estimates based on the morning and afternoon flights with the "optimal" Q_H values (90 and 140 MW) are 712.8 and 384.4 kg/hr, respectively. They are overestimated over the CEMS by 145% and 26%. The CPI Roxboro emission estimates based on the morning flight increase significantly when Q_H is above 100 MW. Overestimation of the SO_2

365   emissions by factors of 18 and 15 are found with Q_H set as 140 and 150 MW, respectively. Table 1 shows that the two heat emissions yield correlation coefficients of 0.10, a significant drop from $r = 0.75$ when Q_H is assumed as 90 MW. Although the

highest correlation coefficient between observations and unit-emission HYSPLIT predictions for a specific flight segment may not produce the best emission estimates, a low correlation coefficient typically indicates modeling deficiencies very effectively.

Table 2. The power plant geolocations, stack heights, and CEMS emissions (United States Environmental Protection Agency (U.S. EPA), 2022).

Power plant	Geolocation	Stack	CEMS SO$_2$ emission (kg/hr)									
name	latitude, longitude	height (m)	13Z	14Z	15Z	16Z	17Z	18Z	19Z	20Z	21Z	22Z
Roxboro	36.483°, -79.073°	122	579	582	582	345	360	509	465	486	508	856
Belews Creek	36.281°, -80.060°	152	1349	1267	1132	943	867	816	772	767	853	1029
CPI Roxboro	36.435°, -78.962°	60	278	306	281	300	279	302	316	295	293	298

Table 3. Estimation of SO$_2$ emissions from the three power plants on March 26, 2019 with 15 different assumed heat emissions and the average CEMS emissions during the specified hours. The ranges of CEMS hourly emissions for the specified hours as well as one hour before and one hour after the period are shown after the average CEMS emission. The relevant CEMS hourly emissions are listed in Table 2. The bold numbers are associated with the heat emissions that generate the highest correlation coefficients between observations and HYSPLIT predictions for the specific flight segments.

CEMS / Assumed	Roxboro		Belews Creek		CPI Roxboro	
heat emission (MW)	15–17Z (kg/hr)	19–20Z (kg/hr)	16–17Z (kg/hr)	18–19Z (kg/hr)	15–16Z (kg/hr)	19–20Z (kg/hr)
CEMS	429 (345–582)	476 (465–509)	905 (816–1132)	794 (767–867)	291 (279–306)	306 (293–316)
10	701.5	449.3	1758.6	680.8	343.1	588.4
20	664.6	532.4	1578.7	512.6	343.8	590.7
30	636.1	530.3	1553.7	424.8	320.5	572.2
40	806.8	740.4	3735.0	339.0	557.5	503.5
50	617.3	491.5	1547.5	339.0	398.5	478.9
60	611.1	506.5	1475.0	283.8	402.5	457.4
70	**551.9**	529.3	1445.9	298.9	464.8	475.1
80	538.9	488.6	**1417.3**	393.0	504.5	429.1
90	520.9	485.7	1451.7	368.7	**712.8**	412.3
100	514.7	**520.9**	1411.6	485.7	1095.3	416.4
110	525.0	515.7	1550.6	*697.3*	1372.7	413.9
120	512.6	564.2	1406.0	1027.4	2186.5	361.4
130	521.9	593.1	1716.9	707.1	2627.7	357.1
140	474.2	789.2	1815.7	818.1	5214.3	**384.4**
150	473.2	875.7	1986.5	926.0	4261.5	401.7

3.3.2 SO$_2$ background

370 With zero background SO$_2$ mixing ratios, the emission estimates based on the "optimal" heat emission are all greater than the CEMS emissions. This indicates that it is necessary to consider the SO$_2$ background mixing ratios. The HYSPLIT simulated mixing ratios are actually the enhancements over the background mixing ratios. As shown in Table 4, there are 810 1-min observations, more than half of the 1503 1-min SO$_2$ observations, not residing in any of the HYSPLIT simulated plumes originated from the three power plants with any of the 15 heat emissions. It has to be noted that the flight patterns could have

375 been better constructed. Sampling upwind as well as downwind or in closed shape flight patterns which enclose the sources (e.g., see Ryoo et al. (2019), Fathi et al. (2021), and Kim et al. (2023)) would have helped significantly in the estimation of the SO$_2$ background mixing ratios.

At first, the median value of the missed SO$_2$ observations (0.199 ppbv) is assumed as the background SO$_2$ mixing ratio. This value is subtracted from all the observations unless the values are below this background value, where the observations are set

380 as zero. Using the adjusted observations, the emission estimations results are listed in Table 5. Compared to the estimates with zero background mixing ratios, the estimated emissions are all reduced, as expected. The Roxboro emissions are estimated to be 436 kg/hr for 15-17Z and 403.3 kg/hr for 19-20Z. Both estimates agree much better with the CEMS than the previous estimates without considering the background SO$_2$ mixing ratios. The estimated Belews Creek emission of 1259.7 kg/hr is significant improved as well. The CPI Roxboro emission during the 15-16Z period is overestimated by 89%, but it is not as

385 severe as the previous 145% overestimation. The estimated CPI Roxboro emission for the 19-20Z period is within 4% of the CEMS value.

Table 4 shows the statistical distribution values of the six different segments, i.e., the morning and afternoon plumes from the three power plants. The highest 1-min SO$_2$ mixing ratio of 7.249 ppbv is inside the Belews Creek plume measured during the morning flight. The observed SO$_2$ mixing ratios inside the Belews Creek plumes are much higher than those from the other

390 plumes. It is beneficial to assume different background values for the six different segments of the observations. The minimum, the 5th percentile, the 10th percentile, and the 25th percentile mixing ratios of the morning and afternoon observations inside the plumes from three different power plants are assumed as segment-specific background mixing ratios. After subtracting the assumed background values from the observations, the emission estimations results are listed in Table 5. The estimated emissions decrease with increasing background values. With the segment-specific 25th percentile as the background, the Belews

395 Creek emission estimation of 929.7 kg/hr is within 3% of the CEMS values and the other estimates are comparable to the results by assuming a constant background mixing ratio of 0.199 ppbv.

3.3.3 Root mean square errors (RMSEs)

Up to now, the best heat emission parameters are selected based on the correlation coefficients between the observations and predicted counterparts for each segment of the observations after an ensemble of HYSPLIT runs with 15 different heat emission

400 are performed. This can be performed before the emissions are estimated since the correlation coefficients are not affected by

Table 4. Number of 1-min SO$_2$ observations and some statistics of the SO$_2$ mixing ratios. There are overlapping between Roxboro and CPI Roxboro segments since some observations are affected by both power plants.

Number of SO$_2$ observations /SO$_2$ mixing ratio (ppbv)	All observations	Roxboro		Belews Creek		CPI Roxboro		Missed observations
		morning	afternoon	morning	afternoon	morning	afternoon	
Number of observations	1503	192	186	55	23	118	153	810
Minimum	0.001	0.002	0.001	0.147	0.011	0.031	0.025	0.001
5th percentile	0.032	0.045	0.032	0.332	0.011	0.051	0.045	0.026
10th percentile	0.058	0.066	0.066	0.589	0.019	0.083	0.094	0.046
25th percentile	0.136	0.128	0.166	1.041	0.038	0.175	0.209	0.114
Median	0.257	0.307	0.398	2.002	0.500	0.297	0.351	0.199
75th percentile	0.465	0.586	0.611	2.826	0.665	0.493	0.538	0.317
Maximum	7.249	2.862	1.626	7.249	3.780	1.578	1.246	1.721

Table 5. Estimation of SO$_2$ emissions from the three power plants on March 26, 2019 with different background mixing ratios. The "optimal" heat emission that generates the highest correlation coefficient between observations and unit-emission HYSPLIT predictions for the specific flight segment is assumed. Complete emission estimates with all heat emissions and different background mixing ratios are listed in Tables 3, A1, A2, A3, A4, and 6. The average CEMS emissions during the specified hours are listed for reference. The relevant CEMS hourly emissions are listed in Table 2. The segment-specific statistical distribution values are listed in Table 4.

CEMS / Background SO$_2$ mixing ratios	Roxboro		Belews Creek	CPI Roxboro	
	15–17Z (kg/hr)	19–20Z (kg/hr)	16–17Z (kg/hr)	15–16Z (kg/hr)	19–20Z (kg/hr)
CEMS	429	476	905	291	306
0	551.9	520.9	1417.3	712.8	384.4
0.199 ppbv	436.0	403.3	1259.7	549.7	294.7
Minimum, segment-specific min	550.8	517.8	1316.3	684.9	371.6
5th percentile, segment-specific	518.8	502.5	1210.3	659.4	359.9
10th percentile, segment-specific	503.5	481.8	1067.2	628.5	335.6
25th percentile, segment-specific	461.1	418.9	929.7	563.1	294.1

the magnitudes of the emissions when emissions for each segment are assumed to be constant. After the emission magnitudes are estimated, model performance can be evaluated using other statistic metrics.

The correlation-based emission estimations using all the 15 different heat emission parameters by assuming the segment-specific 25th percentile observation as the background mixing ratios are listed in Table 6. The root mean square errors (RMSEs) of the HYSPLIT predicted morning and afternoon plumes from the three power plants with all the plume rise ensemble runs

are listed in Table 7. The "optimal" heat emissions that yield the best correlation coefficients also result in the smallest RMSEs for two segments, the morning plumes from Roxboro and Belews Creek. The afternoon plume from Roxboro predicted with $Q_H = 90$ MW and the estimated emission of 389.9 kg/hr has the smallest RMSE of 0.428 ppbv. The emission is underestimated by 18%. However, for both the morning and afternoon plumes from CPI Roxboro, "optimal" heat emissions associated with the highest correlation coefficients are quite different from the heat emissions that produce the smallest RMSEs. If the model runs associated the smallest RMSEs are selected, the estimated CPI Roxboro SO_2 emissions are 265.1 kg/hr for 15-16Z and 389.1 kg/hr for 19–20Z, 9% underestimated and 27% overestimated over CEMS. While the 19–20Z emission is worse than the result based on the best correlation, the 15-16Z emission estimation is much closer to the CEMS than the correlation-based result, which is 94% overestimated. For the plume from the Belews Creek observed during the afternoon flight, $Q_H = 140$ MW yields the least RMSE of 1.874 ppbv, which is more than three times of the median SO_2 observation in the segment. The least RMSE of 0.859 ppbv for the Belews Creek morning segment is smaller than the 25th percentile value of the observation (1.041 ppbv). For all the other four segments, the best RMSEs are slightly larger than the median of the observations. This indicates the poor performance of the Belews Creek afternoon model simulation. However, the emission inversion with $Q_H = 140$ MW still yields a very good estimate of 811.6 kg/hr, which is only 2% overestimated.

Figure 7 shows the comparison of both the RMSE-based and correlation-based optimal predictions with the morning and afternoon flight observations in the HYSPLIT predicted plumes from the three power plants. Identical results are obtained using the smallest RMSE and the highest correlation coefficient for the morning segments from Roxboro and Belews. For both cases, the predicted SO_2 mixing ratios agree well with the observations. Note that here the SO_2 predictions include both the predicted SO_2 enhancement with the estimated emissions and the assumed segment-specific background values which are chosen as the 25th percentile observations inside the particular plumes. For the other cases, the RMSE-based predictions tend to produce lower mixing ratios for the observed high SO_2 values. Thus the linear regression lines for the RMSE-based predictions tend to have flatter slopes. However, the RMSE-based emission can still be larger, such as the CPI Roxboro afternoon case. The scatter plot for the Belews Creek afternoon case clearly shows anti-correlation as indicated by the negative correlation coefficients listed in Table 1. This is caused by plume misplacement due to wind direction errors. Although the predicted high and low mixing ratios are opposite to the observations, the minimization of the cost function defined by Equation 4 is still capable of reaching to an estimate close to the actual emission rate. The observations appear to have a good representation of its mixing ratio distribution for the plume at the distance from the source. Even if the model misplaced the plume location, predicted mixing ratios that have a similar distribution of the low and high values still has the minimal cost function. That is, the inverse modeling method is not very sensitive to the plume misplacement. If $Q_H = 110$ MW that generates the highest negative correlation of -0.68 is chosen as the "optimal" plume rise parameter, the estimated emission for Belews Creek during the 18-19Z period is 709.9 kg/hr, which is only 11% lower than the CEMS value of 794 kg/hr. It might still be possible to have reasonable emission inversion results even when plumes are misplaced by the model.

Figure 8 shows the "optimal" predictions based on the highest correlation coefficients and minimal RMSEs at 800 m above ground level at 17Z and 19Z. Continuous vertical profiles along the flight track, or "curtain" plots, of the correlation-based and RMSE-based "optimal" predictions are shown in Figure 9 and enlarged in Figures 10, and A1– A9. For the morning flight,

Table 6. Estimated SO$_2$ emissions from the three power plants on March 26, 2019 with 15 different assumed heat emissions and the average CEMS emissions during the specified hours. The segment-specific 25th percentile observations are assumed as the background SO$_2$ mixing ratios and have been subtracted from the observations for emission inversion. The ranges of CEMS hourly emissions for the specified hours as well as one hour before and one hour after the period are shown after the average CEMS emission. The relevant CEMS hourly emissions are listed in Table 2. The bold numbers are associated with the heat emissions which generate the highest correlation coefficients between observations and HYSPLIT predictions for the specific flight segments. The underlined numbers are associated with the smallest RMSEs listed in Table 7.

CEMS / Assumed	Roxboro		Belews Creek		CPI Roxboro	
heat emission (MW)	15–17Z (kg/hr)	19–20Z (kg/hr)	16–17Z (kg/hr)	18–19Z (kg/hr)	15–16Z (kg/hr)	19–20Z (kg/hr)
CEMS	429 (345–582)	476 (465–509)	905 (816–1132)	794 (767–867)	291 (279–306)	306 (293–316)
10	609.9	365.7	1290.2	701.5	292.4	481.8
20	576.7	425.7	1165.2	512.6	290.6	495.5
30	545.4	427.4	1121.8	418.9	265.1	483.8
40	674.0	568.7	2606.8	332.9	479.9	420.6
50	531.4	394.6	1077.9	330.3	311.7	389.1
60	517.8	403.3	975.4	272.6	320.5	373.8
70	**461.1**	427.4	935.3	287.8	358.5	395.4
80	445.7	399.3	**929.7**	378.4	394.6	352.8
90	436.9	389.9	948.5	362.1	**563.1**	336.3
100	434.3	**418.9**	913.2	480.9	895.1	353.5
110	436.9	424.0	995.1	*709.9*	1162.9	324.4
120	434.3	467.6	922.3	1062.9	1947.2	282.6
130	454.7	490.6	1097.4	731.5	2509.7	282.1
140	408.2	634.8	1249.6	811.6	5373.0	**294.1**
150	416.4	730.1	1445.9	924.2	3176.9	311.1

the "optimal" predictions of the Roxboro and Belews Creek plumes based on the highest correlation coefficient and minimal RMSE are identical. The prediction results agree well with the observed plume placement and width, as well as the mixing ratios. On the other hand, for the CPI Roxboro morning plume, the RMSE-based "optimal" prediction with $Q_H = 30$ MW is quite different from the correlation-based "optimal" prediction with $Q_H = 90$ MW. The center of the RMSE-based plume is at lower altitude than the correlation-based plume (Figures A1, A2, and A4). The lower-placed plume is also associated with lower mixing ratios that match the observations better. Figure 8(c) shows a wider CPI Roxboro plume of the RMSE-based result than the correlation-based result in Figure 8(a). The larger extent of the RMSE-based CPI Roxboro plume results in an extra appearance of the plume under the flight track in the curtain plot (Figure A3).

445

Table 7. RMSEs of the SO_2 mixing ratios of morning and afternoon plumes from three power plants calculated using the estimated SO_2 emissions from the three power plants with 15 different assumed heat emissions listed in Table 6. Bold numbers are associated with the heat emissions which generate the highest correlation coefficients between observations and unit-emission HYSPLIT predictions for the specific flight segments. The underlined numbers indicate the smallest RMSEs of each segment.

SO_2 RMSE (ppbv) /	Roxboro		Belews Creek		CPI Roxboro	
Assumed heat emission (MW)	morning	afternoon	morning	afternoon	morning	afternoon
10	0.635	0.429	1.409	2.590	0.612	0.538
20	0.640	0.469	1.368	2.140	0.525	0.564
30	0.635	0.486	1.242	2.079	0.438	0.566
40	0.684	0.681	2.706	2.212	1.299	0.984
50	0.539	0.442	1.106	2.520	0.509	0.470
60	0.444	0.478	0.916	2.681	0.464	0.527
70	**0.434**	0.476	0.918	2.412	0.470	0.559
80	0.471	0.431	**0.859**	2.222	0.451	0.522
90	0.455	0.428	1.031	1.916	**0.496**	0.527
100	0.481	**0.456**	1.040	1.905	0.586	0.630
110	0.511	0.488	1.290	*2.334*	0.871	0.630
120	0.563	0.589	1.299	2.879	1.777	0.699
130	0.725	0.652	1.362	2.120	2.679	0.665
140	0.766	0.838	1.590	1.874	4.701	**0.553**
150	0.893	0.866	1.630	1.903	2.956	0.563

For the Roxboro plume captured during the afternoon flight, the correlation-based "optimal" prediction with $Q_H = 100$ MW and SO_2 emission of 418.9 kg/hr shows very similar spatial structures and mixing ratios as the RMSE-based "optimal" prediction with $Q_H = 90$ MW and 389.9 kg/hr. Figure 8, Figure 10, and Figures ~~10~~A7– A9 show little differences between the two and both agree well with the 1-min aircraft observations. Figure 10 show that both predictions underestimated the observed peak values along the flight, but the peak location and the width of the Roxboro plumes match well between the predictions and observations. Note that the SO_2 emission are underestimated by both of the "optimal" selections for this segment.

As shown in Table 1, strong anti-correlation is found between predicted and observed SO_2 mixing ratios of the Belews Creek afternoon plume. The prediction with $Q_H = 110$ MW that has highest absolute correlation coefficient is selected here as the correlation-based solution. Figure A6 shows that it is not very different from the RMSE-based result with $Q_H = 140$ MW. Both cases clearly misplaced the first transect of the plume and predicted wider transects than the observations. It is found that the second transect shown in Figures A6 is well predicted with $Q_H = 110$ MW.

For the CPI Roxboro plume observed during the afternoon flight, the correlation-based "optimal" prediction with $Q_H = 140$ MW and the RMSE-based "optimal" prediction with $Q_H = 50$ MW appear drastically different in Figure 8, Figure 10, and
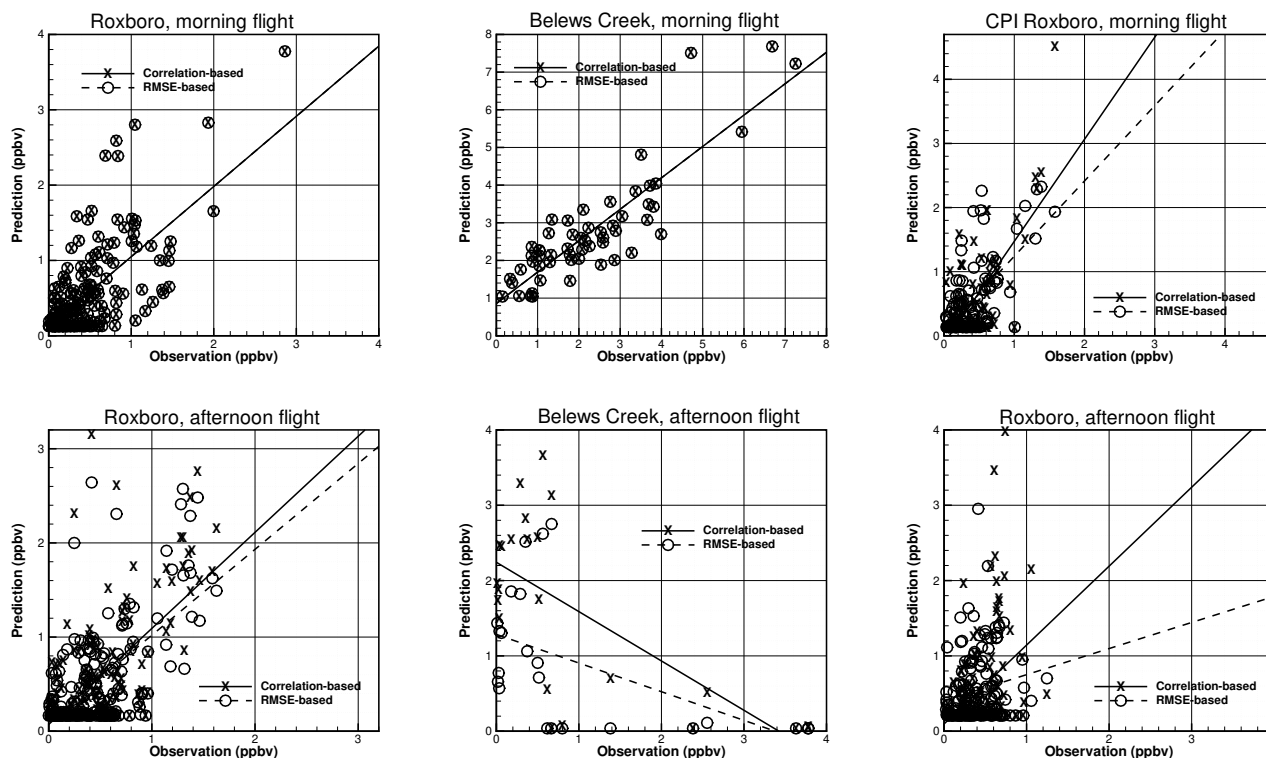
Figure 7. Comparison of the correlation-based and the RMSE-based "optimal" predictions with the morning and afternoon flight observations in the HYSPLIT predicted SO$_2$ plumes from the three power plants. The correlation-based predictions are with the Q$_H$ values which generate the highest correlation coefficients listed in Table 1. The highest absolute correlation coefficient is selected for the Belews Creek afternoon flight case. The RMSE-based predictions are associated with the cases which generate the smallest RMSEs listed in Table 7. The linear regression lines are shown for both the correlation-based and the RMSE-based predictions with the observations.

Figures 10A7– A9, as expected. Figures 10 Figure 10 and Figures A7– A9 show that the RMSE-based "optimal" prediction has wider plume transects and have them placed at lower altitudes than the correlation-based results. The predicted mixing ratios match the observations much better than the correlation-based results although the estimated emission of 389.1 kg/hr is not

465   closer to the CEMS emission of 306 kg/hr than the correlation-based estimation of 294.1 kg/hr. In addition, Figure 10 shows that the RMSE-based solution captures an observed narrow CPI Roxboro plume transect that correlation-based solution fails to reproduce. The results here indicate the need to have more observations at different altitudes in the future flight planning.

4   Summary and discussion

An ensemble of HYSPLIT runs with various heat release parameters for the Briggs plume rise algorithm are made to estimate

470   SO$_2$ emissions from three power plants. Using a TCM approach for the inverse modeling, independent HYSPLIT Lagrangian
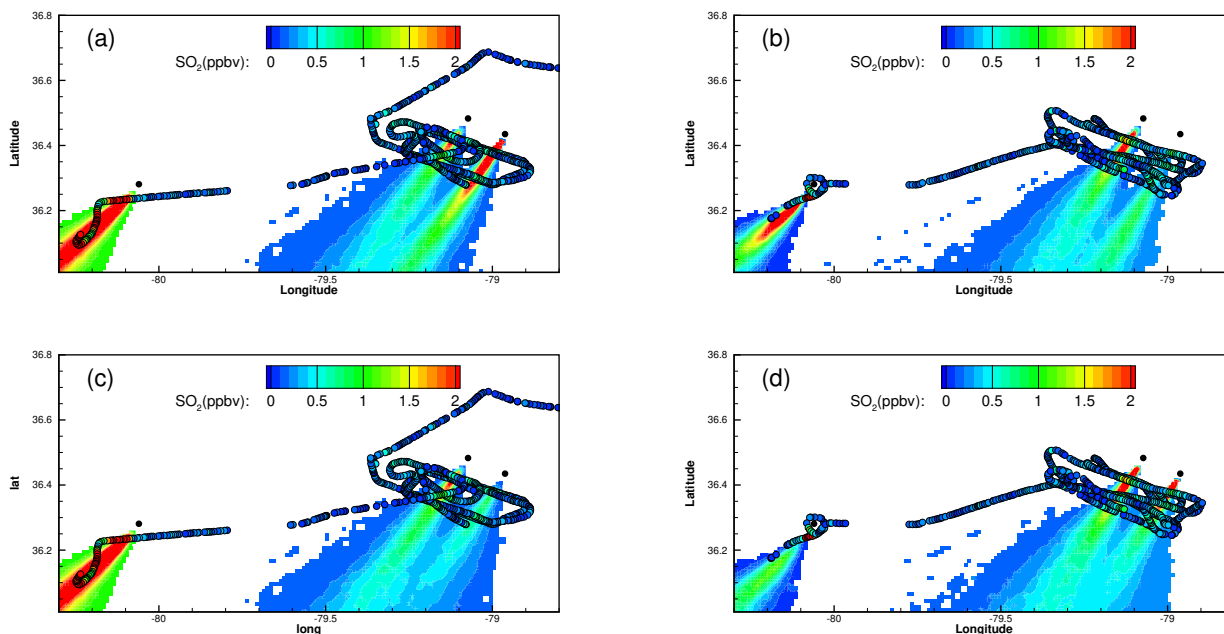
Figure 8. Comparison of the correlation-based (a, b) and the RMSE-based (c, d) "optimal" predictions at 800 m above ground level at 17:00Z (a, c) and 19:00Z (b, d). The morning (a, c) and afternoon (b, d) 1-min observations are overlaid as circles. Color indicates the SO_2 values for both predictions and observations. The three power plants are marked with solid black circles.

model runs with unit hourly emissions are carried out for each heat release value. The SO_2 emissions from the three power plants during the morning and afternoon flight periods on March 26, 2019 are estimated separately through six different segments.

Initially the "optimal" plume rise runs are selected based on the highest correlation coefficients between predictions and

475 observations. A segment with negative correlations is excluded. It is found that the SO_2 emissions are overestimated for all the remaining segments if background mixing ratios are not considered. Several different assumptions of background values are then tested. Assuming the 25th percentile observed SO_2 mixing ratio inside each segment as the background SO_2 mixing ratios yields good emission estimates, with the relative errors as 18%, -12%, 3%, 93.5%, and -4% when compared with the CEMS data (see Figure 11). Note that the ranges of the inverted emissions with 10 MW above and below the "optimal" heat

480 emissions are used to indicate the sensitivities of the results to the heat emissions. While the differences between the emission estimates and the known CEMS data provide some confidence to the results, quantification of the uncertainties associated with the method probably requires further investigation in the future.

Using the same segment-specific SO_2 background assumption, "optimal" plume rise runs are later selected to have the smallest RMSEs between the predicted and observed mixing ratios. The previously excluded segment that has negative correlation

485 coefficients between predictions and observations is also included in the emission inversion. While identical plume rise runs
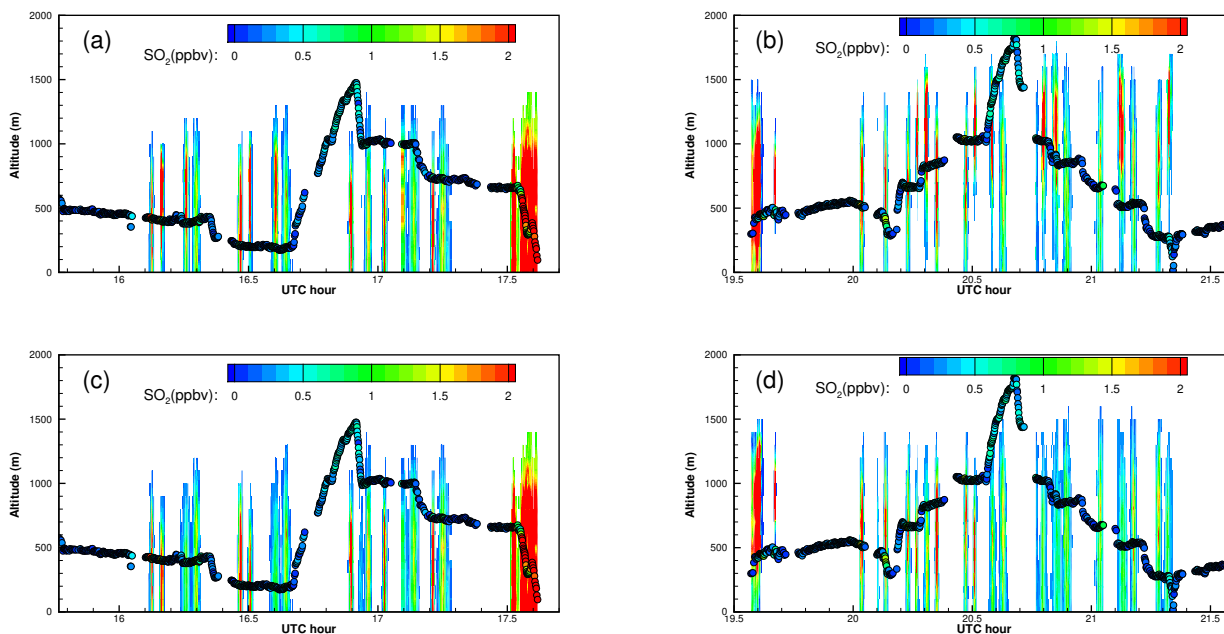
Figure 9. "Curtain" plots of the correlation-based (a, b) and the RMSE-based (c, d) "optimal" predictions. In the "curtain" plots, continuous vertical profiles along the flight track are shown following the observation time. The morning (a, c) and afternoon (b, d) 1-min observations are overlaid as circles. Color indicates the SO_2 values for both predictions and observations.

are chosen as the "optimal" members for Roxboro and Belews Creek morning segments, different runs are selected for the other three segments than the previous correlation-based results. In addition, emission inversion for the previously excluded segment that has negative correlation coefficients between predictions and observations is also carried out. The relative errors as 18%, -18%, 3%, -9%, and 27% for the five segments, and 2% for the Belews Creek afternoon segment. Figure 11 shows that the RMSE-based estimate of SO_2 emission from CPI Roxboro at 15–16 Z agrees much better with the CEMS data than the correlation-based estimate does. The RMSE-based SO_2 emission estimates of Roxboro at 19–20 Z and CPI Roxboro at 19–20 Z appear to deteriorate slightly. However, the associated HYSPLIT predictions show better agreement with the observations than the correlation-based "optimal" runs because of their smaller RMSEs.

While the stack exit gas temperature data are not available for this study, a single constant stack exit temperature is provided for each facility in the 2020 National Emissions Inventory (NEI) (Personal communication with George Pouliot at the U.S. EPA). Using the average measured air temperature as the ambient temperature and the other CEMS data (United States Environmental Prote , including hourly exit air flow rates, the morning/afternoon heat emissions are estimated as 52–59 MW/49–56 MW, 80–92 MW/76–87 MW, and 13–13 MW/12–13 MW, for Roxboro, Belews Creek, and CPI Roxboro, respectively. Note that the heat emission estimation is sensitive to the stack exit temperature which is expected to vary from hour to hour, similar to the exit air flow rates, and the SO_2 emissions. Nonetheless, these estimated values indicate the reasonable ranges of the heat emission. When

correlation-based and RMSE-based methods agree with each other in their "optimal" heat emission for Roxboro and Belews Creek morning segments, the "optimal" heat emissions are very close to the estimated stack heat emissions here. When the two methods disagree, the correlation-based "optimal" heat emissions of 90 MW/140 MW for CPI Roxboro morning/afternoon are unreasonably high, but the RMSE-based "optimal" emissions of 30 MW/50 MW could still be reasonable. This suggests that

505   the RMSE-based results are probably more reliable.

While the uncertainty of the heat emission is focused here, there are a lot of other uncertainties associated with the emission estimates. For instance, uncertainties in many parameters, such as the assumed background SO_2 mixing ratios, the meteorological data input ~~and~~ such as the wind direction and speed, and some of the HYSPLIT turbulence parameterizations ~~. The inverse modeling results also depend on the assumed background SO_2 mixingratios and several uncertainty parameters used~~

510   ~~in the cost function formula. Additional analyses could be carried out, but will not be included here .~~ related to the turbulent mixing, will all affect the final results. Even if the hourly exit temperature were available, the plume rise calculated using the Briggs algorithm may still misplace the plume. It is likely that the "optimal" heat emissions chosen here have compensated other errors in the model.

The relative low resolution of heat emission with an increment of 10 MW for the plume rise ensemble runs may result in

515   significant errors for some cases. For instance, Figure 11 shows large ranges of the emission estimates when using 10 MW above and below the correlation-based and RMSE-based "optimal" heat emissions for the CPI Roxboro afternoon segment. Since it is not easy to select the best performance plume rise run based on the limited observations, it is probably better to use several ensemble members to quantify the uncertainties of the model simulation as well as the emission estimates. This is indicated in Figure 11, but needs to be further explored in the future.

520   Negative correlation is found between predictions and observations for the Belews Creek plume captured by the afternoon flight due to the wind direction errors of the meteorological data. However, the RMSE-based SO_2 emission estimate is only 2% above the CEMS value. More surprisingly, if the plume rise run with the highest absolute correlation coefficient is selected, the SO_2 estimate of 715.6 kg/hr is very close to the CEMS average emission rate of 794 kg/hr. We speculate that the inverse modeling is not very sensitive to the plume misplacement because the cost function minimization would favor an unbiased

525   population distribution even when misplacement by the model is present. However, special care is needed for such situations where large RMSEs indicate the model deficiencies.

It has to be noted that the current dispersion simulation directly places the pollutant release points with the calculated plume rises elevated above the stacks while the actual plumes reach their apexes gradually. Thus the dispersion model is not able to accurately reproduce the exact plume shapes at locations close to the source. The afternoon flight around Belews Creek power

530   plant is closer to the source than the other segments. This probably makes this case more difficult to simulate accurately than the other segments.

This study shows that RMSE is a better metric than correlation coefficient in choosing the best ensemble member for the SO_2 emission inversion. While the RMSE-based "optimal" plume rise runs appear to agree better with the observations than the correlation-based "optimal" runs, observations are often missing when and where the "optimal" runs are significantly

535   different. Additional measurements at multiple altitudes would have been really helpful. In the future flight planning of similar

top-down emission estimation studies more vertical profiles of the target pollutant should be measured. In addition, more upwind measurements are also recommended in order to better quantify the background concentrations caused by many other emission sources. It is also wise to choose relative steady meteorological conditions for the flight campaign since the unsteady conditions such as frequent wind direction changes pose great challenges not only to the inverse modeling but also to the
540   meteorological simulation and the dispersion modeling. The current study shows the value of the ensemble simulations when certain model parameters are difficult to determine, such as stack heat emission here.

Code and data availability. HYSPLIT code is available at https://www.ready.noaa.gov/HYSPLIT.php. The observation data are available upon request.

Author contributions. TC designed and performed the model analysis, and wrote the first draft of the paper. XR conducted the measurement
545   collection and analysis. FN completed the WRF runs to generate meteorological data. MC provided expertise for the HYSPLIT modeling and plume rise algorithm. AC conducted the initial SO_2 simulations. All authors contributed to the paper editing and revision.

Competing interests. The authors have declared that there are no competing interests.

Acknowledgements. This study was supported by NOAA Award NA16OAR4590121 at the NOAA Air Resources Laboratory in collaboration with the Cooperative Institute for Satellites Earth System Studies (CISESS), University of Maryland, College Park, MD 20740, USA

Table A1. Estimated SO$_2$ emissions from the three power plants on March 26, 2019 with 15 different assumed heat emissions and the average CEMS emissions during the specified hours. A constant 0.199 ppbv background SO$_2$ mixing ratio is assumed and has been subtracted from the observations for emission inversion. The ranges of CEMS hourly emissions for the specified hours as well as one hour before and one hour after the period are shown after the average CEMS emission. The relevant CEMS hourly emissions are listed in Table 2. The bold numbers are associated with the heat emissions which generate the highest correlation coefficients between observations and HYSPLIT predictions for the specific flight segments. The underlined numbers are associated with the smallest RMSEs listed in Table 7.

CEMS / Assumed	Roxboro		Belews Creek		CPI Roxboro	
heat emission (MW)	15–17Z (kg/hr)	19–20Z (kg/hr)	16–17Z (kg/hr)	18–19Z (kg/hr)	15–16Z (kg/hr)	19–20Z (kg/hr)
CEMS	429 (345–582)	476 (465–509)	905 (816–1132)	794 (767–867)	291 (279–306)	306 (293–316)
10	584.9	352.1	1556.8	1249.6	293.6	478.0
20	547.5	412.3	1397.6	922.3	288.9	491.5
30	519.8	416.4	1383.7	668.6	262.0	478.9
40	637.3	542.1	3333.0	452.0	471.3	415.6
50	513.6	382.9	1361.7	446.6	311.7	386.0
60	494.5	389.9	1300.6	335.6	317.3	370.9
70	**436.0**	413.1	1274.9	362.1	350.7	392.2
80	423.1	386.8	**1259.7**	556.4	388.3	348.6
90	427.4	376.8	1282.5	460.2	**549.7**	334.3
100	419.8	**403.3**	1247.1	590.7	886.2	350.7
110	416.4	410.6	1375.4	*973.5*	1151.4	323.1
120	421.5	455.6	1237.2	1808.5	1958.9	283.2
130	449.3	478.0	1504.8	4561.0	2606.8	282.1
140	409.0	614.8	1620.3	888.0	5682.1	**294.7**
150	417.3	708.5	1772.7	916.8	3267.0	311.1

Table A2. Estimated SO$_2$ emissions from the three power plants on March 26, 2019 with 15 different assumed heat emissions and the average CEMS emissions during the specified hours. The segment-specific minimum observations are assumed as the background SO$_2$ mixing ratios and have been subtracted from the observations for emission inversion. The ranges of CEMS hourly emissions for the specified hours as well as one hour before and one hour after the period are shown after the average CEMS emission. The relevant CEMS hourly emissions are listed in Table 2. The bold numbers are associated with the heat emissions which generate the highest correlation coefficients between observations and HYSPLIT predictions for the specific flight segments. The underlined numbers are associated with the smallest RMSEs listed in Table 7.

CEMS / Assumed	Roxboro		Belews Creek		CPI Roxboro	
heat emission (MW)	15–17Z (kg/hr)	19–20Z (kg/hr)	16–17Z (kg/hr)	18–19Z (kg/hr)	15–16Z (kg/hr)	19–20Z (kg/hr)
CEMS	429 (345–582)	476 (465–509)	905 (816–1132)	794 (767–867)	291 (279–306)	306 (293–316)
10	700.1	448.4	1626.8	721.4	330.3	569.9
20	664.6	530.3	1463.3	537.8	330.3	576.7
30	634.8	527.2	1443.0	443.0	308.6	557.5
40	802.0	735.9	3503.7	350.7	541.0	488.6
50	617.3	488.6	1428.6	350.7	380.6	463.9
60	609.9	503.5	1361.7	291.2	383.7	443.9
70	**550.8**	527.2	1337.5	307.4	443.0	462.9
80	536.7	485.7	**1316.3**	407.4	481.8	416.4
90	518.8	482.8	1345.5	380.6	**684.9**	400.9
100	511.6	**517.8**	1308.4	499.5	1058.7	406.6
110	523.0	514.7	1443.0	_725.7_	1342.8	403.3
120	507.5	562.0	1300.6	1086.5	2147.5	352.1
130	517.8	590.7	1585.1	758.3	2575.7	347.9
140	468.5	784.5	1699.9	843.0	5214.3	**371.6**
150	468.5	873.9	1856.1	952.3	4127.4	387.5
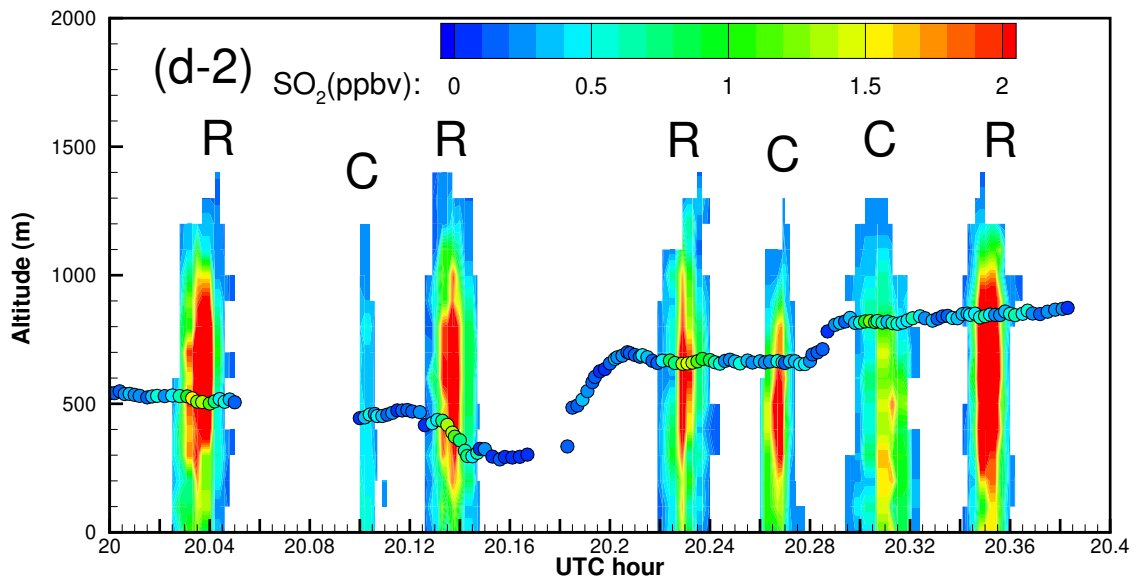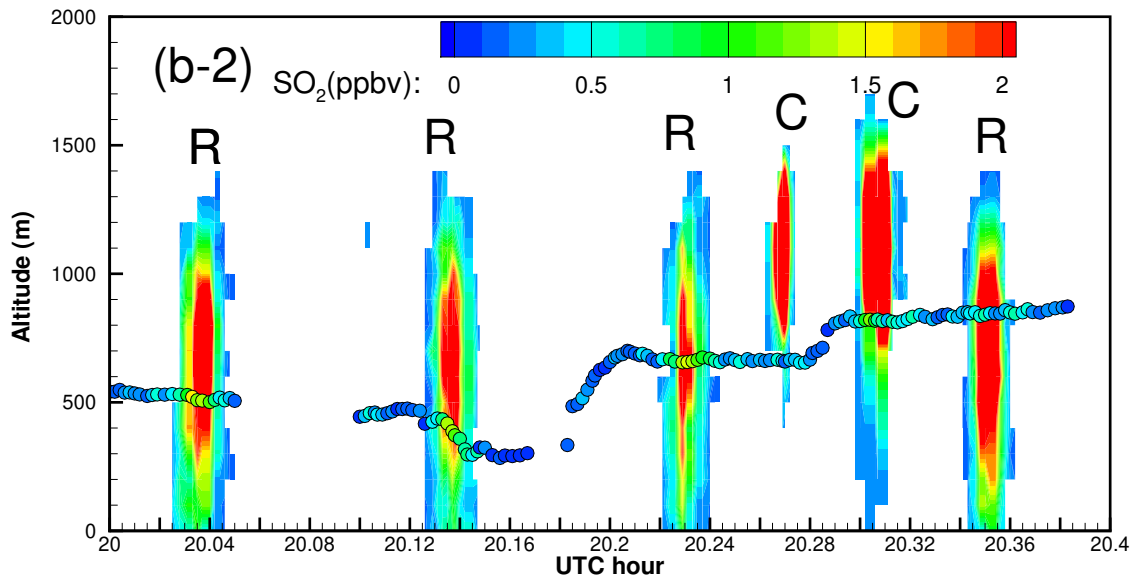
Figure 10. Enlarged "curtain" plots of the correlation-based (b) and the RMSE-based (d) "optimal" predictions in Figure 9 (Part 2). In the "curtain" plots, continuous vertical profiles along the flight track are shown following the observation time. The afternoon flight 1-min observations are overlaid as circles. Color indicates the SO_2 values for both predictions and observations. Predicted plumes from Roxboro, Belews Creek, and CPI Roxboro are indicated with letters "R", "B", and "C", respectively.
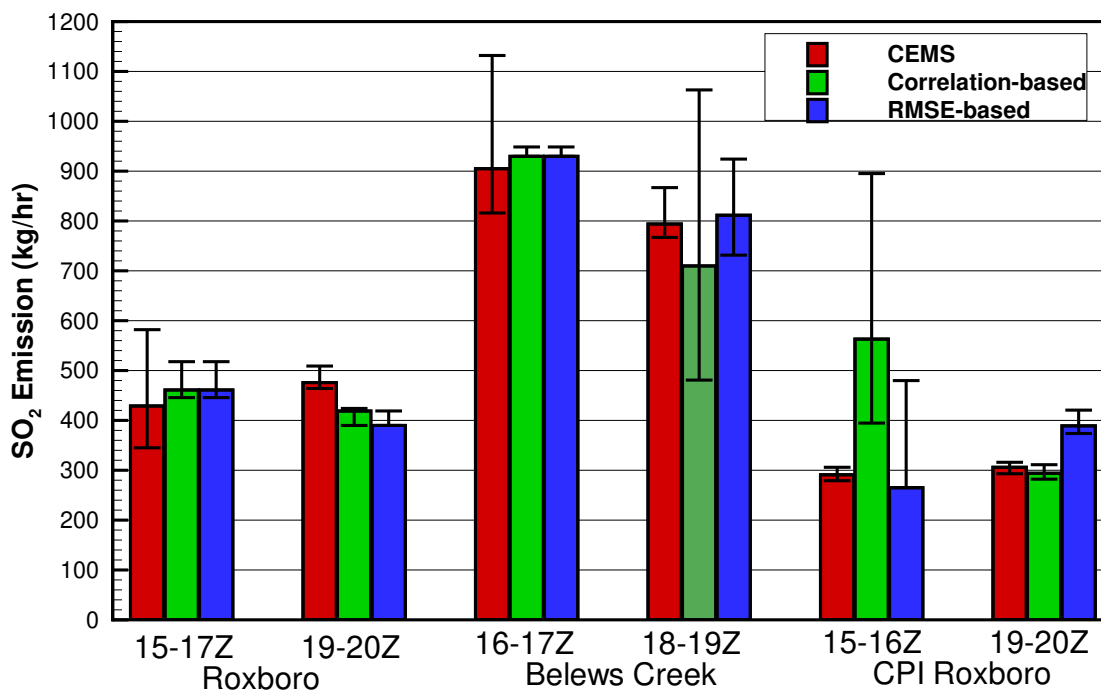
Figure 11. The CEMS and estimated SO$_2$ emissions from the three power plants on March 26, 2019 during the specified hours. Error bars of CEMS emissions indicate the ranges of hourly emissions for the specified hours as well as one hour before and one hour after. Correlation-based and RMSE-based estimates are the inversion results using the "optimal" heat emission that generates the highest correlation coefficient and the smallest RMSE between observations and the HYSPLIT predications for the specific flight segment, respectively. The correlation-based Belews Creek afternoon segment is based on the highest absolute correlation coefficient. Error bars of the estimated SO$_2$ emissions show the ranges of the results using 10 MW above and below the "optimal" heat emissions.

Table A3. Estimated SO_2 emissions from the three power plants on March 26, 2019 with 15 different assumed heat emissions and the average CEMS emissions during the specified hours. The segment-specific 5th percentile observations are assumed as the background SO_2 mixing ratios and have been subtracted from the observations for emission inversion. The ranges of CEMS hourly emissions for the specified hours as well as one hour before and one hour after the period are shown after the average CEMS emission. The relevant CEMS hourly emissions are listed in Table 2. The bold numbers are associated with the heat emissions which generate the highest correlation coefficients between observations and HYSPLIT predictions for the specific flight segments. The underlined numbers are associated with the smallest RMSEs listed in Table 7.

CEMS / Assumed heat emission (MW)	Roxboro		Belews Creek		CPI Roxboro	
	15–17Z (kg/hr)	19–20Z (kg/hr)	16–17Z (kg/hr)	18–19Z (kg/hr)	15–16Z (kg/hr)	19–20Z (kg/hr)
CEMS	429 (345–582)	476 (465–509)	905 (816–1132)	794 (767–867)	291 (279–306)	306 (293–316)
10	668.6	433.4	1489.9	701.5	320.5	550.8
20	638.6	511.6	1334.8	523.0	318.6	560.8
30	603.9	509.5	1329.5	430.8	298.3	542.1
40	752.3	701.5	3326.3	342.4	523.0	473.2
50	589.6	470.4	1300.6	342.4	365.0	447.5
60	581.4	485.7	1244.7	284.3	368.7	430.0
70	**518.8**	511.6	1217.6	300.1	424.8	449.3
80	506.5	470.4	**1210.3**	395.4	462.0	402.5
90	487.6	466.7	1227.4	371.6	**659.4**	388.3
100	485.7	**502.5**	1191.1	490.6	1017.2	393.8
110	494.5	498.5	1316.3	*711.4*	1292.8	390.6
120	481.8	545.4	1179.3	1058.7	2092.4	341.7
130	495.5	573.3	1437.2	731.5	2474.8	337.6
140	446.6	756.8	1566.2	828.0	5090.8	**359.9**
150	448.4	849.8	1723.8	937.2	3895.0	375.3

Table A4. Estimated SO$_2$ emissions from the three power plants on March 26, 2019 with 15 different assumed heat emissions and the average CEMS emissions during the specified hours. The segment-specific 10th percentile observations are assumed as the background SO$_2$ mixing ratios and have been subtracted from the observations for emission inversion. The ranges of CEMS hourly emissions for the specified hours as well as one hour before and one hour after the period are shown after the average CEMS emission. The relevant CEMS hourly emissions are listed in Table 2. The bold numbers are associated with the heat emissions which generate the highest correlation coefficients between observations and HYSPLIT predictions for the specific flight segments. The underlined numbers are associated with the smallest RMSEs listed in Table 7.

CEMS / Assumed heat emission (MW)	Roxboro		Belews Creek		CPI Roxboro	
	15–17Z (kg/hr)	19–20Z (kg/hr)	16–17Z (kg/hr)	18–19Z (kg/hr)	15–16Z (kg/hr)	19–20Z (kg/hr)
CEMS	429 (345–582)	476 (465–509)	905 (816–1132)	794 (767–867)	291 (279–306)	306 (293–316)
10	655.4	415.6	1329.5	708.5	309.8	514.7
20	623.5	490.6	1186.4	525.0	306.8	526.1
30	589.6	487.6	1191.1	431.7	284.9	507.5
40	733.0	666.0	3107.9	342.4	488.6	442.2
50	572.2	452.0	1146.8	341.7	344.4	417.3
60	565.3	463.9	1088.7	283.2	352.1	400.9
70	**503.5**	489.6	1065.0	298.9	401.7	422.3
80	488.6	452.0	**1067.2**	393.8	436.9	376.1
90	472.3	446.6	1071.4	371.6	**628.5**	364.3
100	472.3	**481.8**	1033.6	490.6	969.6	371.6
110	478.9	479.9	1126.3	*715.6*	1242.2	365.0
120	468.5	525.0	1021.3	1069.3	2030.7	321.2
130	485.7	551.9	1247.1	741.8	2411.4	316.1
140	435.1	725.7	1367.2	828.0	5020.1	**335.6**
150	436.9	821.4	1519.9	939.1	3624.7	352.8
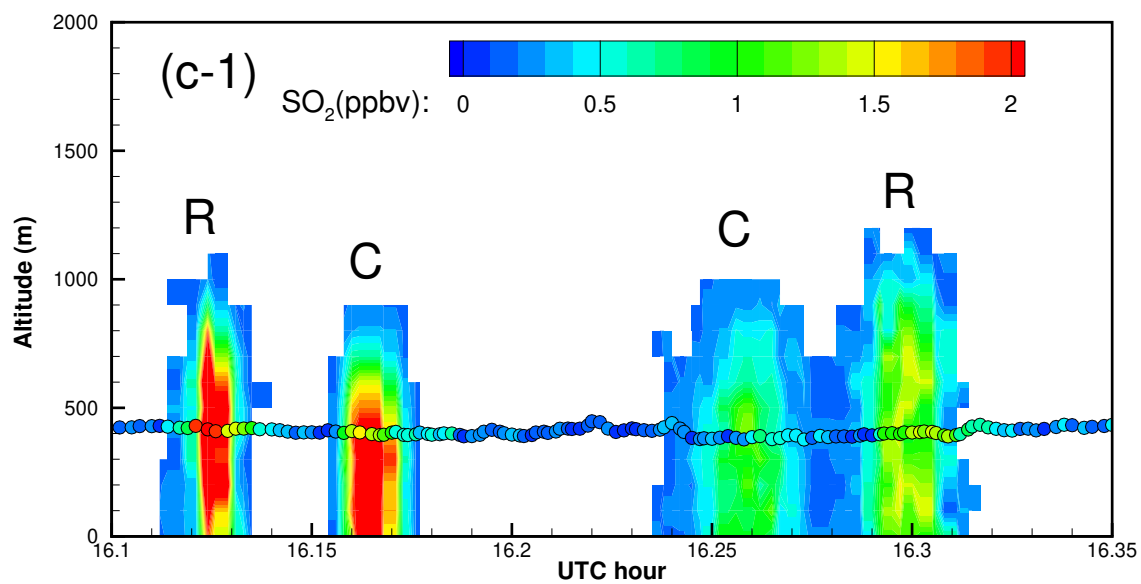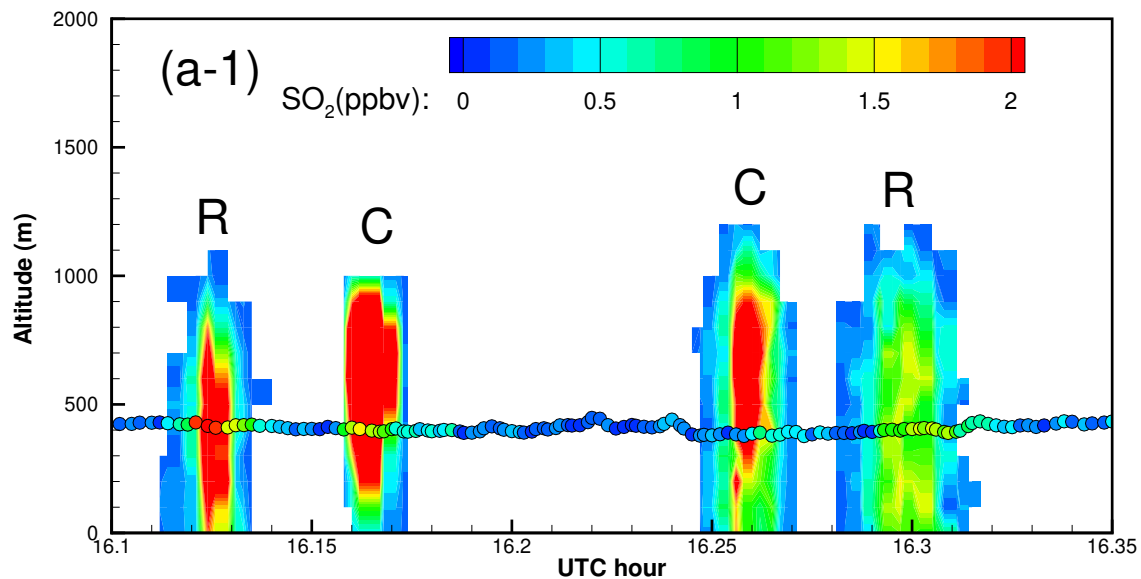
Figure A1. Enlarged "curtain" plots of the correlation-based (a) and the RMSE-based (c) "optimal" predictions in Figure 9 (Part 1). In the "curtain" plots, continuous vertical profiles along the flight track are shown following the observation time. The morning flight 1-min observations are overlaid as circles. Color indicates the SO_2 values for both predictions and observations. Predicted plumes from Roxboro, Belews Creek, and CPI Roxboro are indicated with letters "R", "B", and "C", respectively.
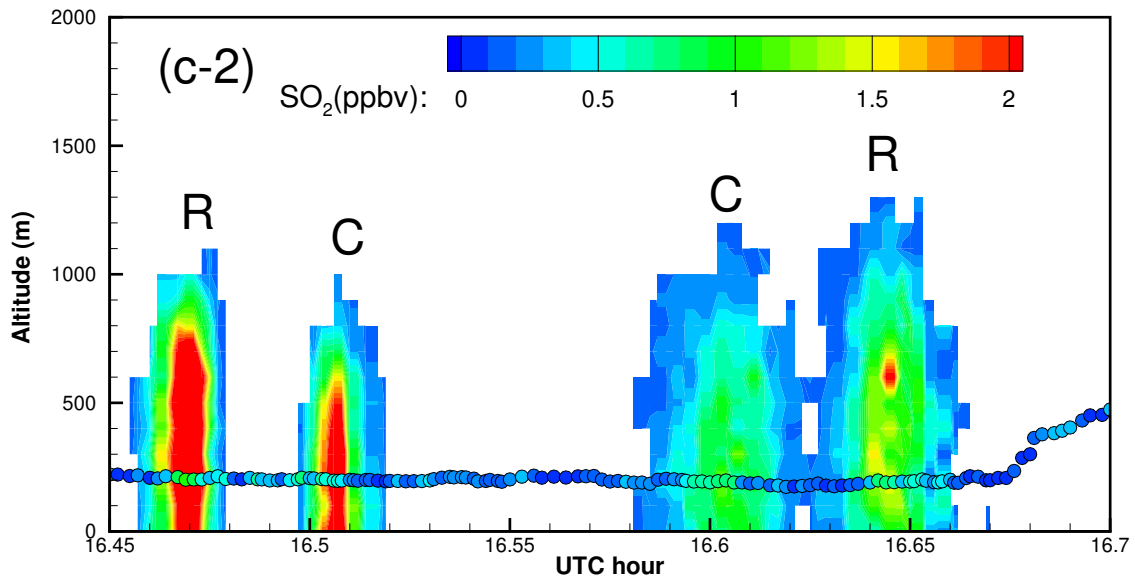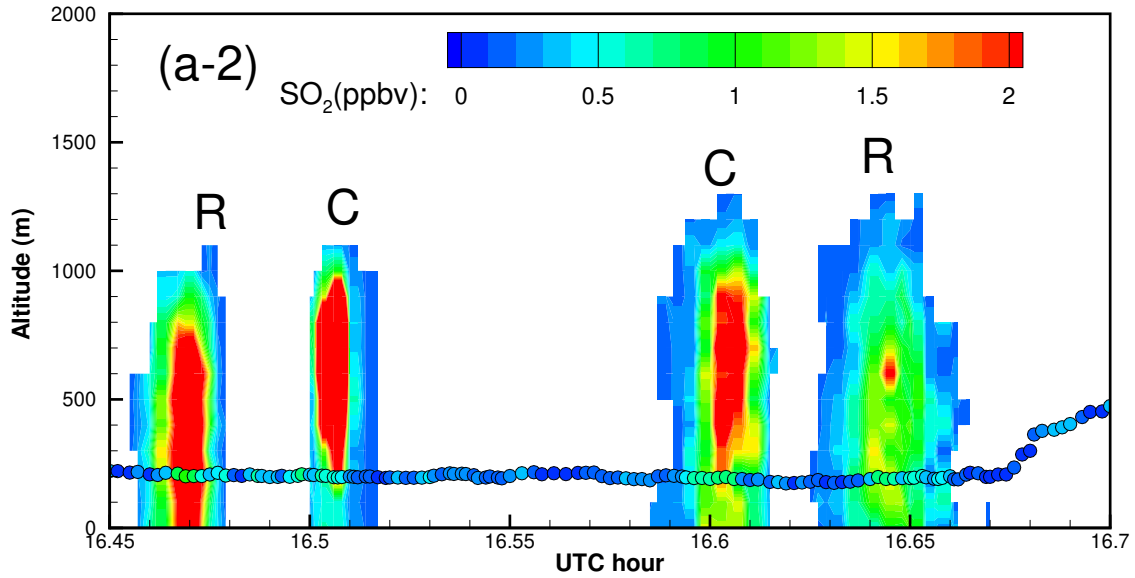
Figure A2. Enlarged "curtain" plots of the correlation-based (a) and the RMSE-based (c) "optimal" predictions in Figure 9 (Part 2). In the "curtain" plots, continuous vertical profiles along the flight track are shown following the observation time. The morning flight 1-min observations are overlaid as circles. Color indicates the SO_2 values for both predictions and observations. Predicted plumes from Roxboro, Belews Creek, and CPI Roxboro are indicated with letters "R", "B", and "C", respectively.
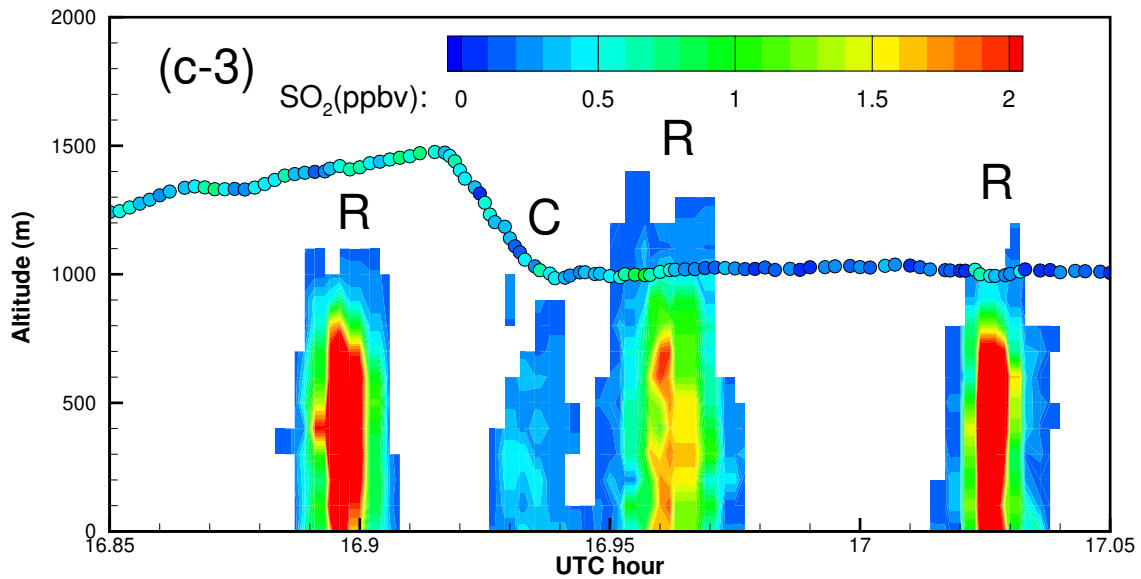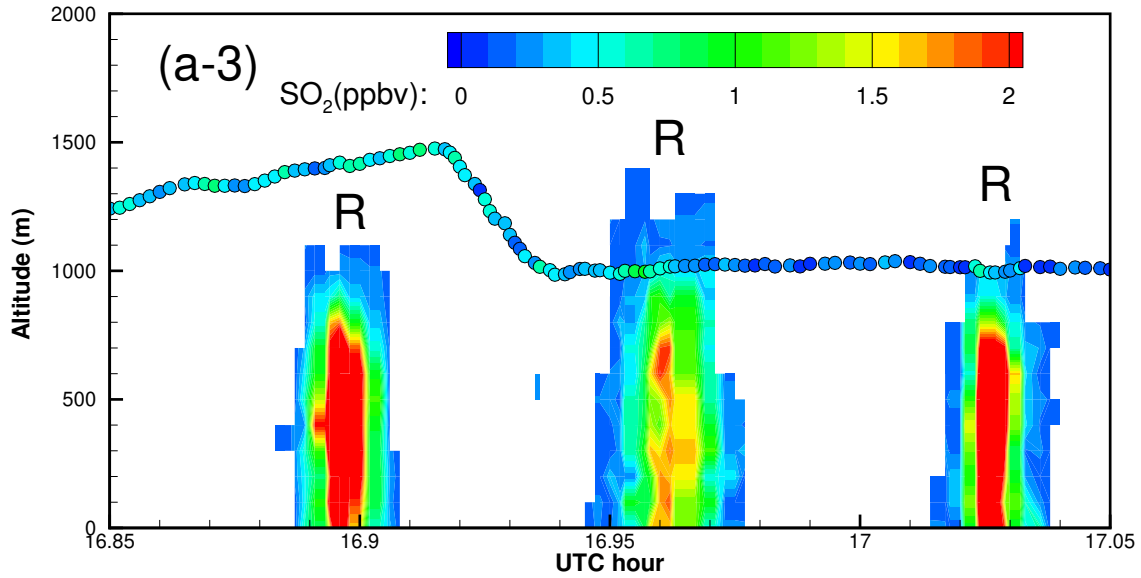
Figure A3. Enlarged "curtain" plots of the correlation-based (a) and the RMSE-based (c) "optimal" predictions in Figure 9 (Part 3). In the "curtain" plots, continuous vertical profiles along the flight track are shown following the observation time. The morning flight 1-min observations are overlaid as circles. Color indicates the SO_2 values for both predictions and observations. Predicted plumes from Roxboro, Belews Creek, and CPI Roxboro are indicated with letters "R", "B", and "C", respectively.
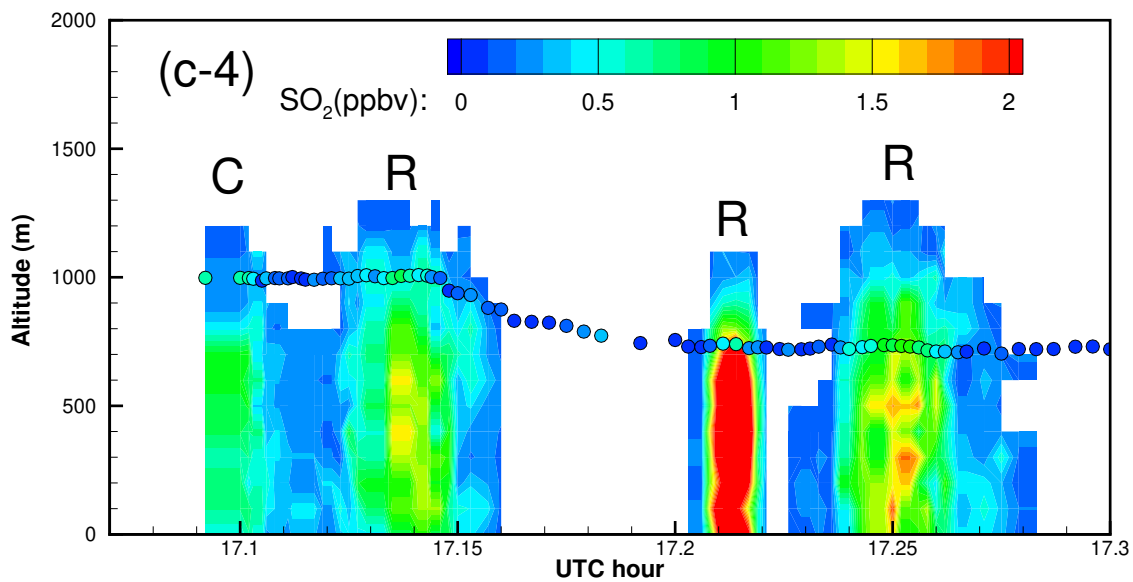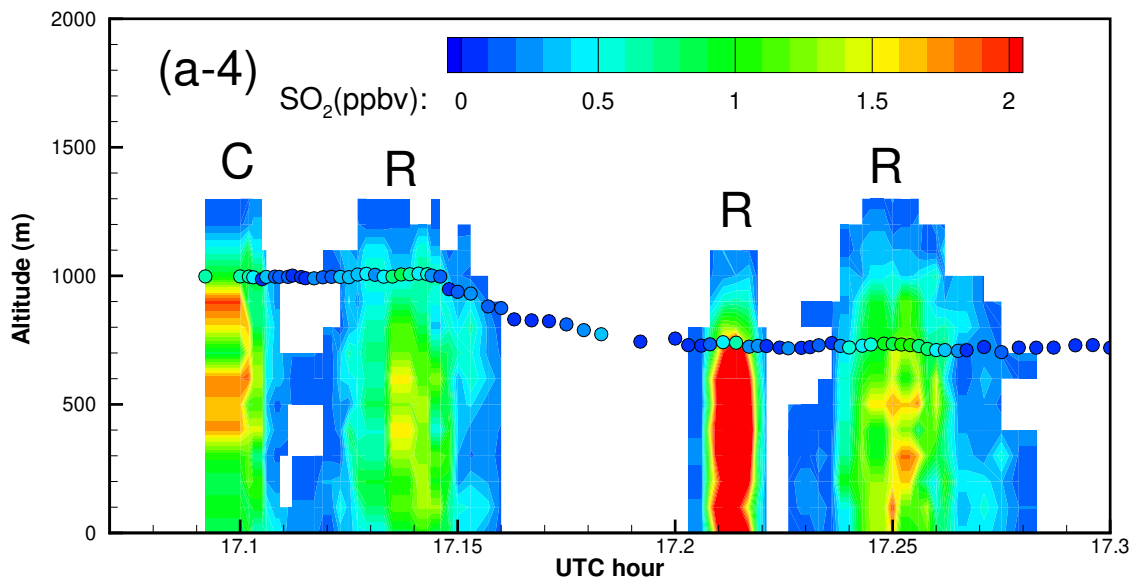
Figure A4. Enlarged "curtain" plots of the correlation-based (a) and the RMSE-based (c) "optimal" predictions in Figure 9 (Part 4). In the "curtain" plots, continuous vertical profiles along the flight track are shown following the observation time. The morning flight 1-min observations are overlaid as circles. Color indicates the SO_2 values for both predictions and observations. Predicted plumes from Roxboro, Belews Creek, and CPI Roxboro are indicated with letters "R", "B", and "C", respectively.
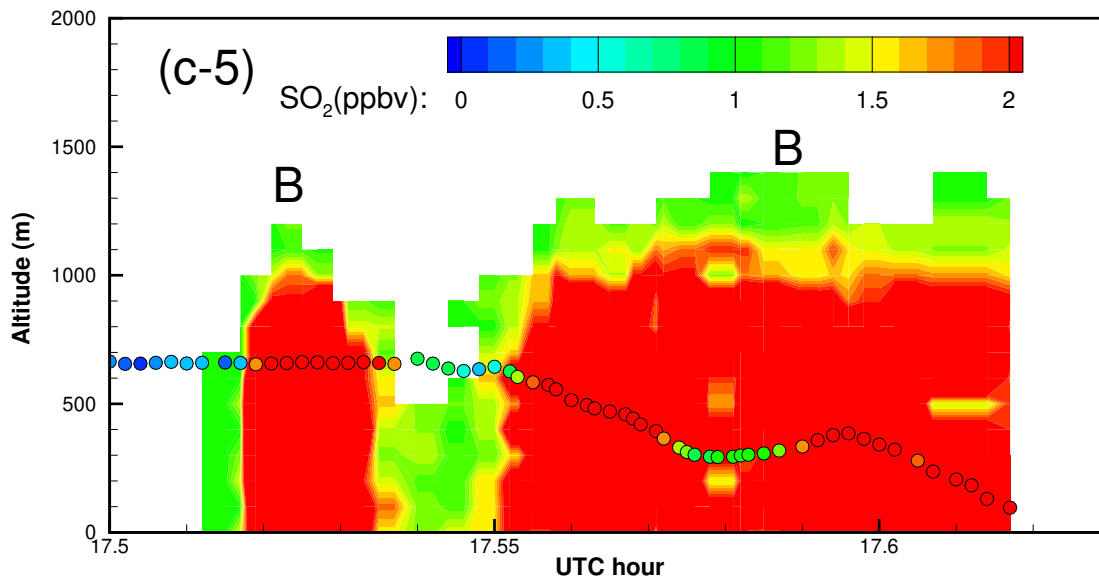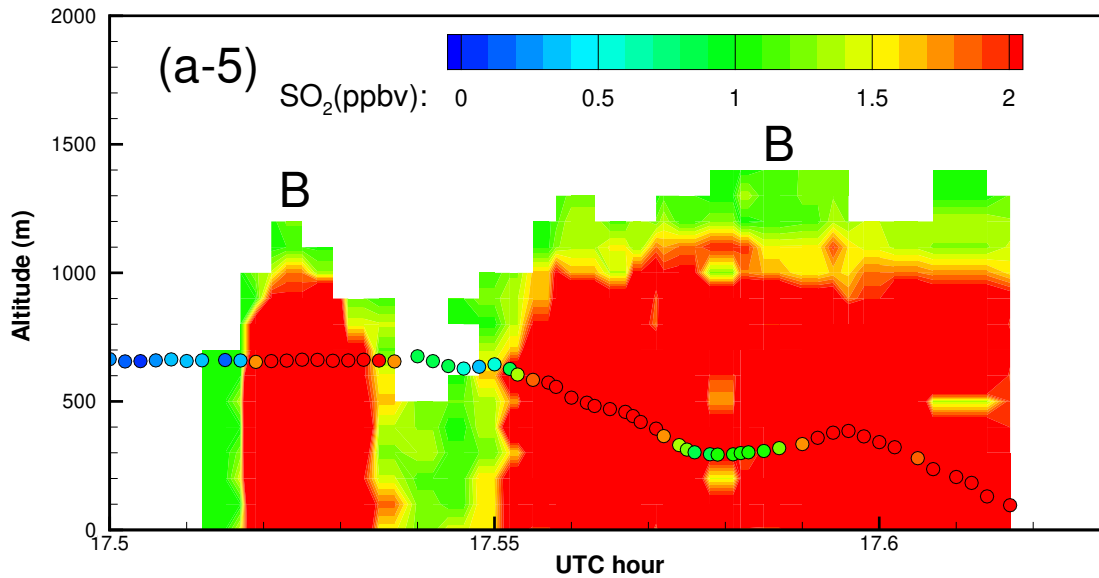
Figure A5. Enlarged "curtain" plots of the correlation-based (a) and the RMSE-based (c) "optimal" predictions in Figure 9 (Part 5). In the "curtain" plots, continuous vertical profiles along the flight track are shown following the observation time. The morning flight 1-min observations are overlaid as circles. Color indicates the SO₂ values for both predictions and observations. Predicted plumes from Roxboro, Belews Creek, and CPI Roxboro are indicated with letters "R", "B", and "C", respectively.
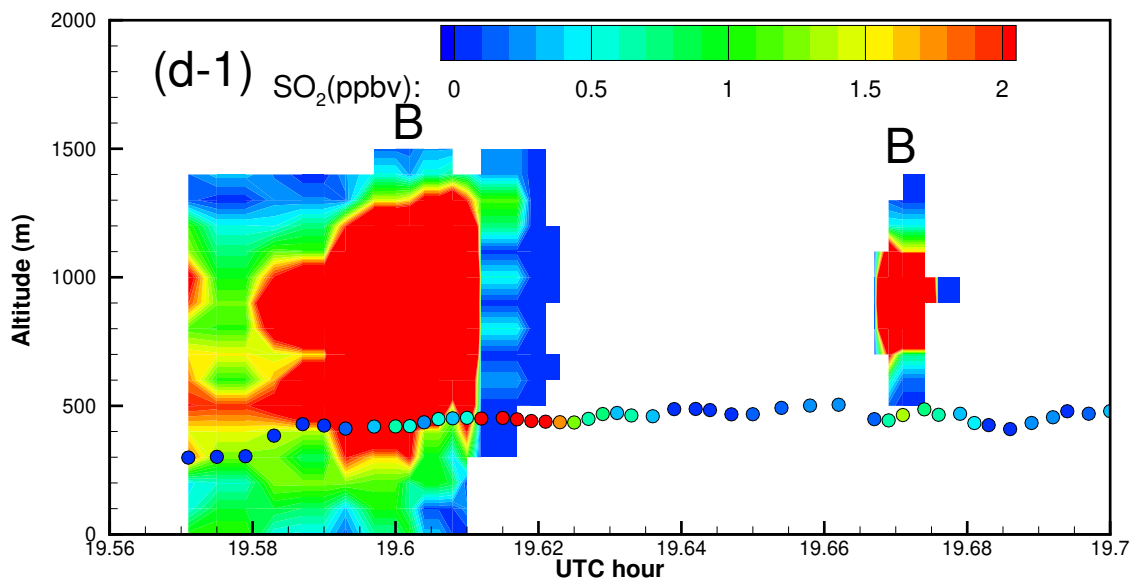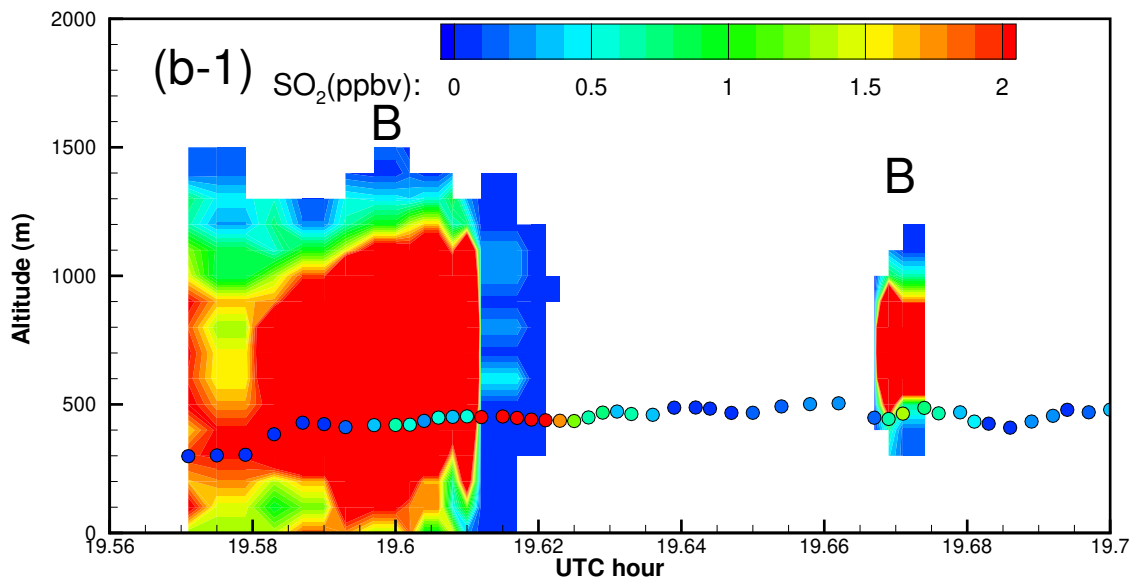
Figure A6. Enlarged "curtain" plots of the correlation-based (b) and the RMSE-based (d) "optimal" predictions in Figure 9 (Part 1). In the "curtain" plots, continuous vertical profiles along the flight track are shown following the observation time. The afternoon flight 1-min observations are overlaid as circles. Color indicates the SO_2 values for both predictions and observations. Predicted plumes from Roxboro, Belews Creek, and CPI Roxboro are indicated with letters "R", "B", and "C", respectively.
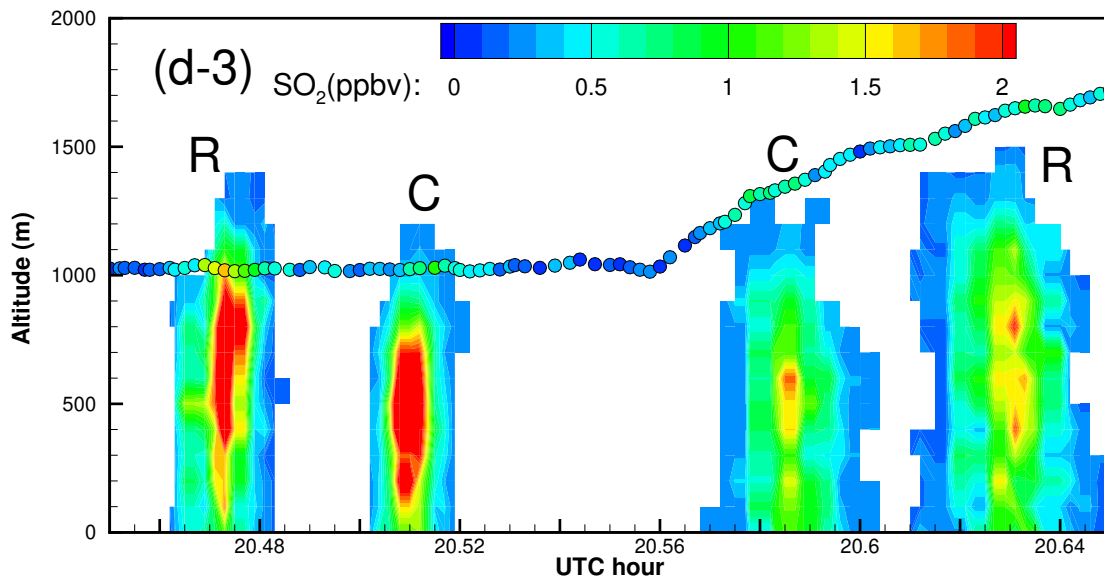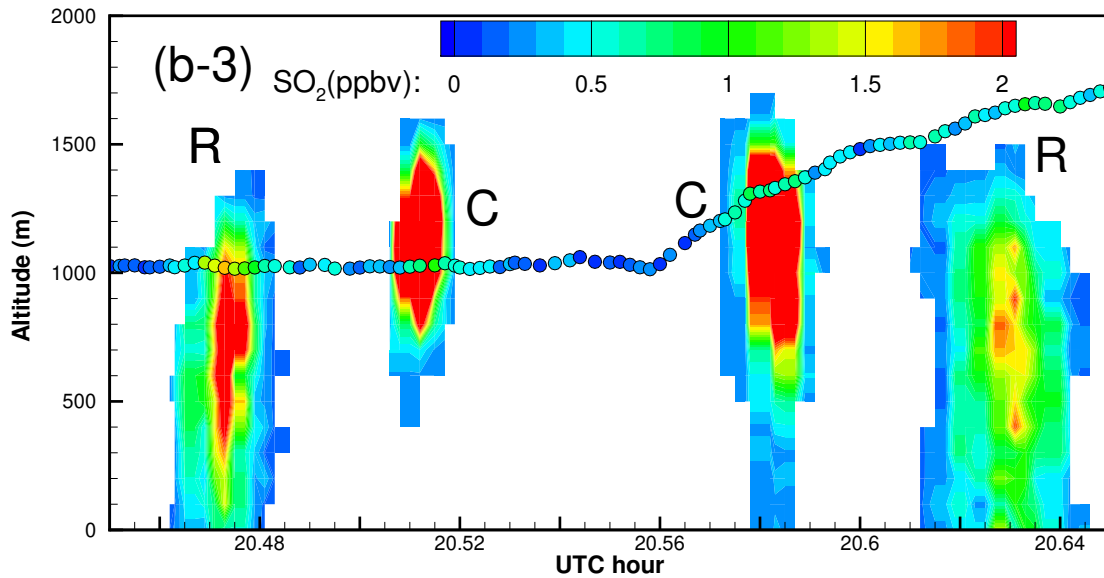
Figure A7. Enlarged "curtain" plots of the correlation-based (b) and the RMSE-based (d) "optimal" predictions in Figure 9 (Part 3). In the "curtain" plots, continuous vertical profiles along the flight track are shown following the observation time. The afternoon flight 1-min observations are overlaid as circles. Color indicates the SO_2 values for both predictions and observations. Predicted plumes from Roxboro, Belews Creek, and CPI Roxboro are indicated with letters "R", "B", and "C", respectively.
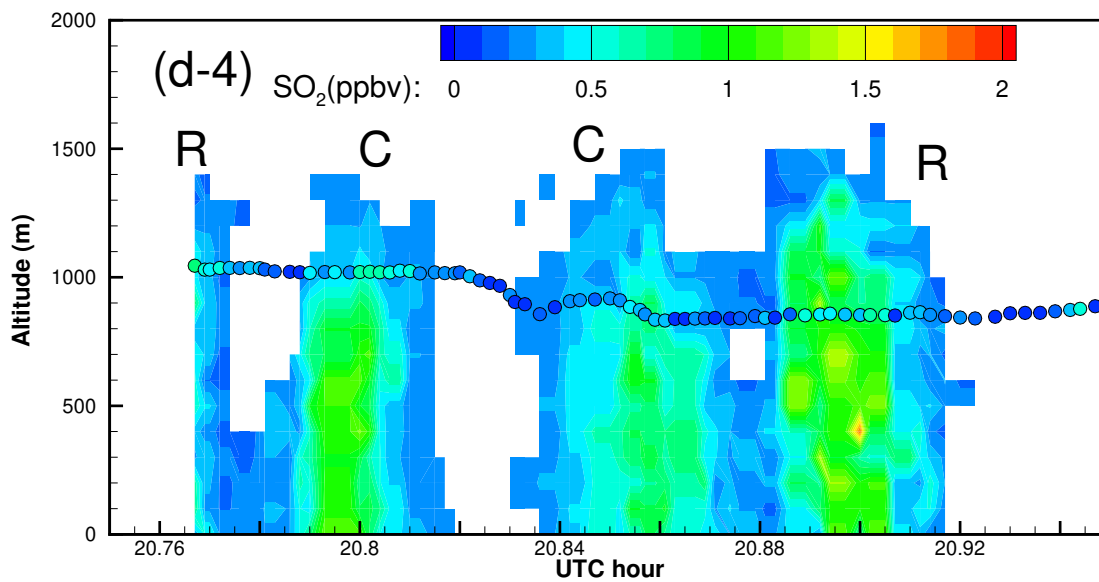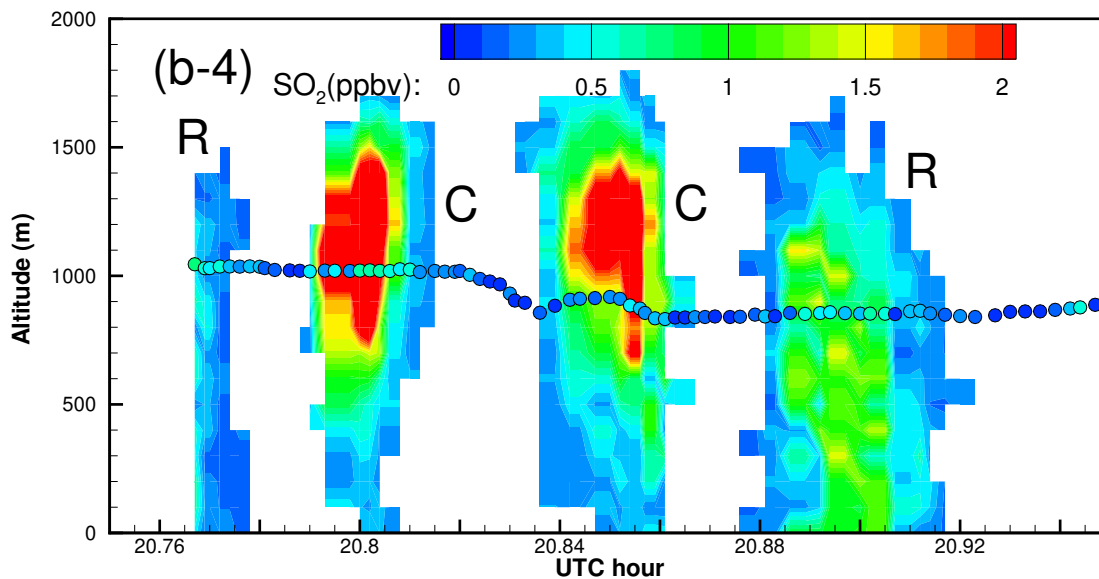
Figure A8. Enlarged "curtain" plots of the correlation-based (b) and the RMSE-based (d) "optimal" predictions in Figure 9 (Part 4). In the "curtain" plots, continuous vertical profiles along the flight track are shown following the observation time. The afternoon flight 1-min observations are overlaid as circles. Color indicates the SO_2 values for both predictions and observations. Predicted plumes from Roxboro, Belews Creek, and CPI Roxboro are indicated with letters "R", "B", and "C", respectively.
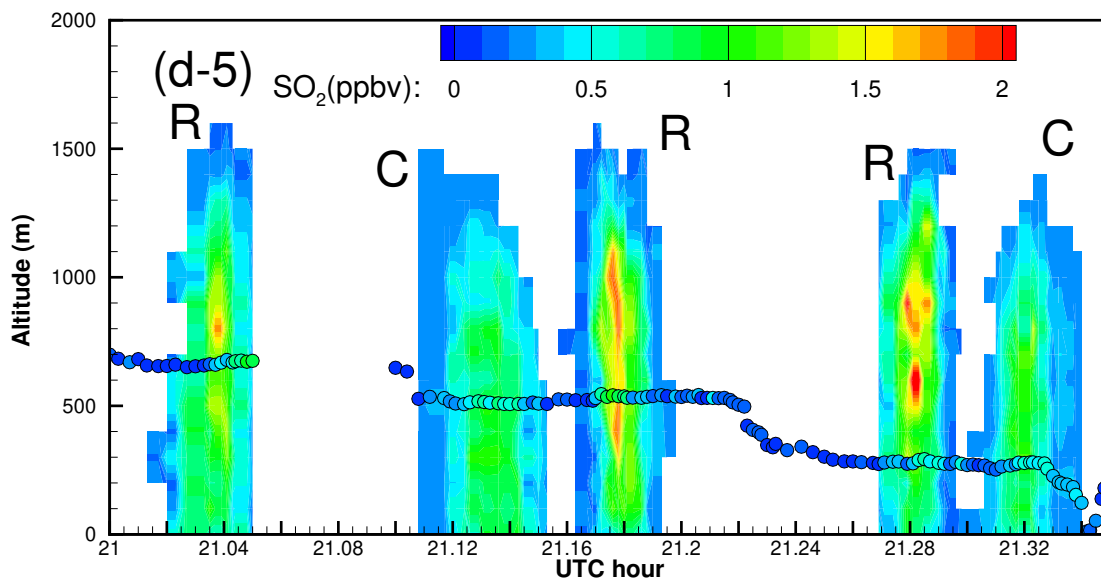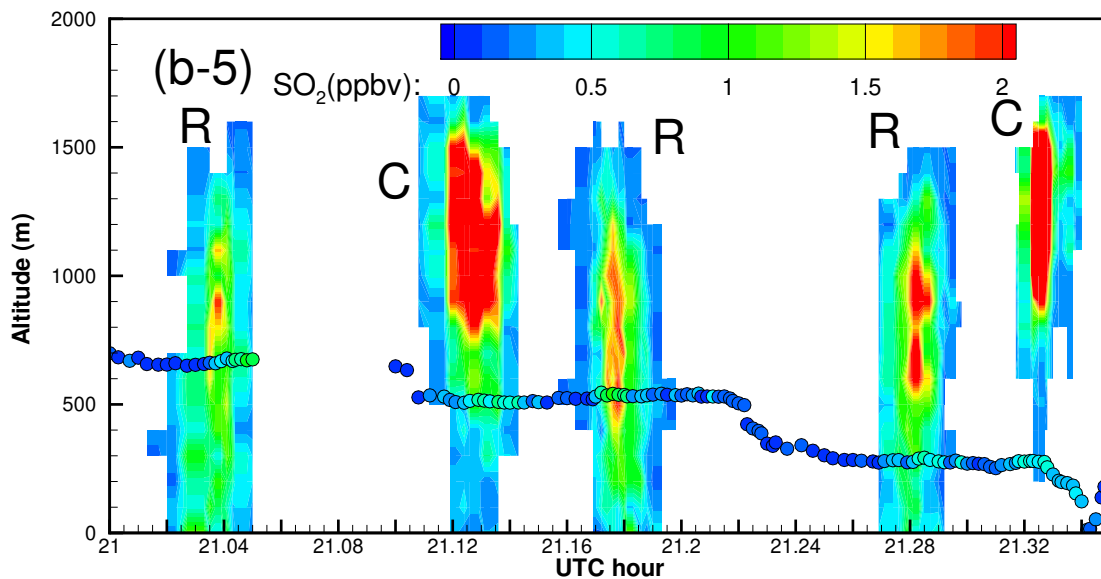
Figure A9. Enlarged "curtain" plots of the correlation-based (b) and the RMSE-based (d) "optimal" predictions in Figure 9 (Part 5). In the "curtain" plots, continuous vertical profiles along the flight track are shown following the observation time. The afternoon flight 1-min observations are overlaid as circles. Color indicates the SO$_2$ values for both predictions and observations. Predicted plumes from Roxboro, Belews Creek, and CPI Roxboro are indicated with letters "R", "B", and "C", respectively.

References

Akingunola, A., Makar, P. A., Zhang, J., Darlington, A., Li, S.-M., Gordon, M., Moran, M. D., and Zheng, Q.: A chemical transport model study of plume-rise and particle size distribution for the Athabasca oil sands, Atmos. Chem. Phys., 18, 8667–8688, https://doi.org/10.5194/acp-18-8667-2018, 2018.

555 Angevine, W. M., Peischl, J., Crawford, A., Loughner, C. P., Pollack, I. B., and Thompson, C. R.: Errors in top-down estimates of emissions using a known source, Atmos. Chem. Phys., 20, 11 855–11 868, https://doi.org/10.5194/acp-20-11855-2020, 2020.

Arya, S. P.: Air pollution meteorology and dispersion, Oxford University Press, New York, NY, 1999.

Bieringer, P. E., Young, G. S., Rodriguez, L. M., Annunzio, A. J., Vandenberghe, F., and Haupt, S. E.: Paradigms and commonalities in atmospheric source term estimation methods, Atmos. Environ., 156, 102 – 112, https://doi.org/10.1016/j.atmosenv.2017.02.011, 2017.

560 Briggs, G. A.: Plume Rise, AEC Critical Review Series TID-25075, U.S. Atomic Energy Commission, Division of Technical Information, Oak Ridge, Tennessee, 1969.

Briggs, G. A.: Plume rise and buoyancy effects, in: Atmospheric Sciences and Power Production, edited by Randerson, D., DOE/TIC-27601 (DE84005177), pp. 327–366, United States Dept. of Energy Technical information Center, Springfield, VA, USA, 1984.

Cambaliza, M. O. L., Shepson, P. B., Caulton, D. R., Stirm, B., Samarov, D., Gurney, K. R., Turnbull, J., Davis, K. J., Possolo, A., Karion,
565 A., Sweeney, C., Moser, B., Hendricks, A., Lauvaux, T., Mays, K., Whetstone, J., Huang, J., Razlivanov, I., Miles, N. L., and Richardson, S. J.: Assessment of uncertainties of an aircraft-based mass balance approach for quantifying urban greenhouse gas emissions, Atmos. Chem. Phys., 14, 9029–9050, https://doi.org/10.5194/acp-14-9029-2014, 2014.

Chai, T., Crawford, A., Stunder, B., Pavolonis, M. J., Draxler, R., and Stein, A.: Improving volcanic ash predictions with the HYSPLIT dispersion model by assimilating MODIS satellite retrievals, Atmos. Chem. Phys., 17, 2865–2879, https://doi.org/10.5194/acp-17-2865-
570 2017, 2017.

Chai, T., Stein, A., and Ngan, F.: Weak-constraint inverse modeling using HYSPLIT-4 Lagrangian dispersion model and Cross-Appalachian Tracer Experiment (CAPTEX) observations – effect of including model uncertainties on source term estimation, Geosci. Model Dev., 11, 5135–5148, https://doi.org/10.5194/gmd-11-5135-2018, 2018.

Chai, T., Draxler, R., and Stein, A.: Source term estimation using air concentration measurements and a Lagrangian dispersion model
575 - Experiments with pseudo and real cesium-137 observations from the Fukushima nuclear accident, Atmos. Environ., 106, 241–251, https://doi.org/10.1016/j.atmosenv.2015.01.070, 2015.

Chang, J. S., Middleton, P. B., Stockwell, W. R., Binkowski, F. S., and Byun, D.: The regional acid deposition model and engineering model, in: Acidic deposition: State of science and technology, Vol I, Emissions, Atmospheric Processes, and Deposition, PB-92-100403/XAB, USA, https://www.osti.gov/biblio/5388896, 1990.

580 Chen, F. and Dudhia, J.: Coupling an advanced land surface-hydrology model with the Penn State-NCAR MM5 modeling system. Part I: Model implementation and sensitivity, Monthly Weather Review, 129, 569–585, 2001.

Crawford, A., Chai, T., Wang, B., Ring, A., Stunder, B., Loughner, C. P., Pavolonis, M., and Sieglaff, J.: Evaluation and bias correction of probabilistic volcanic ash forecasts, Atmos. Chem. Phys., 22, 13 967–13 996, https://doi.org/10.5194/acp-22-13967-2022, 2022.

Daley, R.: Atmospheric Data Analysis, Cambridge University Press, Cambridge, 1991.

585 Draxler, R. and Hess, G.: Description of the HYSPLIT_4 modeling system, Tech. Rep. NOAA Technical Memo ERL ARL-224, National Oceanic and Atmospheric Administration, Air Resources Laboratory, Silver Spring, Maryland, USA, 1997.

Draxler, R. and Hess, G.: An overview of the HYSPLIT_4 modeling system for trajectories, dispersion and deposition, Aust. Meteor. Mag., 47, 295–308, 1998.

Fathi, S., Gordon, M., Makar, P. A., Akingunola, A., Darlington, A., Liggio, J., Hayden, K., and Li, S.-M.: Evaluating the impact of storage-and-release on aircraft-based mass-balance methodology using a regional air-quality model, Atmos. Chem. Phys., 21, 15461–15491, https://doi.org/10.5194/acp-21-15461-2021, 2021.

Gordon, M., Makar, P. A., Staebler, R. M., Zhang, J., Akingunola, A., Gong, W., and Li, S.-M.: A comparison of plume rise algorithms to stack plume measurements in the Athabasca oil sands, Atmos. Chem. Phys., 18, 14695–14714, https://doi.org/10.5194/acp-18-14695-2018, 2018.

Green, J. R., Fiddler, M. N., Holloway, J. S., Fibiger, D. L., McDuffie, E. E., Campuzano-Jost, P., Schroder, J. C., Jimenez, J. L., Weinheimer, A. J., Aquino, J., Montzka, D. D., Hall, S. R., Ullmann, K., Shah, V., Jaegle, L., Thornton, J. A., Bililign, S., and Brown, S. S.: Rates of Wintertime Atmospheric SO2 Oxidation based on Aircraft Observations during Clear-Sky Conditions over the Eastern United States, J. of Geophys. Res., 124, 6630–6649, https://doi.org/10.1029/2018JD030086, 2019.

Grell, G. and Devenyi, D.: A generalized approach to parameterizing convection combining ensemble and data assimilation techniques, Geophys. Res. Lett., 29, https://doi.org/10.1029/2002GL015311, 2002.

Hutchinson, M., Oh, H., and Chen, W.-H.: A review of source term estimation methods for atmospheric dispersion events using static or mobile sensors, Information Fusion, 36, 130–148, https://doi.org/10.1016/j.inffus.2016.11.010, 2017.

Iacono, M. J., Delamere, J. S., Mlawer, E. J., Shephard, M. W., Clough, S. A., and Collins, W. D.: Radiative forcing by long-lived greenhouse gases: Calculations with the AER radiative transfer models, J. of Geophys. Res., 113, https://doi.org/10.1029/2008JD009944, 2008.

Karion, A., Lauvaux, T., Lopez Coto, I., Sweeney, C., Mueller, K., Gourdji, S., Angevine, W., Barkley, Z., Deng, A., Andrews, A., Stein, A., and Whetstone, J.: Intercomparison of atmospheric trace gas dispersion models: Barnett Shale case study, Atmos. Chem. Phys., 19, 2561–2576, https://doi.org/10.5194/acp-19-2561-2019, 2019.

Kim, H. C., Chai, T., Stein, A., and Kondragunta, S.: Inverse modeling of fire emissions constrained by smoke plume transport using HYSPLIT dispersion model and geostationary satellite observations, Atmos. Chem. Phys., 20, 10259–10277, https://doi.org/10.5194/acp-20-10259-2020, 2020.

Kim, J., Seo, B.-k., Lee, T., Kim, J., Kim, S., Bae, G.-N., and Lee, G.: Airborne estimation of SO2 emissions rates from a coal-fired power plant using two top-down methods: A mass balance model and Gaussian footprint approach, Sci. Total Environ., 855, https://doi.org/10.1016/j.scitotenv.2022.158826, 2023.

Liggio, J., Li, S.-M., Hayden, K., Taha, Y. M., Stroud, C., Darlington, A., Drollette, B. D., Gordon, M., Lee, P., Liu, P., Leithead, A., Moussa, S. G., Wang, D., O'Brien, J., Mittermeier, R. L., Brook, J. R., Lu, G., Staebler, R. M., Han, Y., Tokarek, T. W., Osthoff, H. D., Makar, P. A., Zhang, J., Plata, D. L., and Gentner, D. R.: Oil sands operations as a large source of secondary organic aerosols, NATURE, 534, 91+, https://doi.org/10.1038/nature17646, 2016.

Lim, K.-S. S. and Hong, S.-Y.: Development of an Effective Double-Moment Cloud Microphysics Scheme with Prognostic Cloud Condensation Nuclei (CCN) for Weather and Climate Models, Monthly Weather Review, 138, 1587–1612, https://doi.org/10.1175/2009MWR2968.1, 2010.

Lopez-Coto, I., Ren, X., Karion, A., McKain, K., Sweeney, C., Dickerson, R. R., McDonald, B. C., Ahn, D. Y., Salawitch, R. J., He, H., Shepson, P. B., and Whetstone, J. R.: Carbon Monoxide Emissions from the Washington, DC, and Baltimore Metropolitan Area: Recent Trend and COVID-19 Anomaly, Environ. Sci. Technol., 56, 2172–2180, https://doi.org/10.1021/acs.est.1c06288, pMID: 35080873, 2022.

Mays, K. L., Shepson, P. B., Stirm, B. H., Karion, A., Sweeney, C., and Gurney, K. R.: Aircraft-Based Measurements of the Carbon Footprint of Indianapolis, Environ. Sci. Technol., 43, 7816–7823, https://doi.org/10.1021/es901326b, pMID: 19921899, 2009.

Mesinger, F., DiMego, G., Kalnay, E., Mitchell, K., Shafran, P., Ebisuzaki, W., Jovic, D., Woollen, J., Rogers, E., Berbery, E., Ek, M., Fan, Y., Grumbine, R., Higgins, W., Li, H., Lin, Y., Manikin, G., Parrish, D., and Shi, W.: North American regional reanalysis, Bull. Amer. Meteorol. Soc., 87, 343–360, https://doi.org/10.1175/BAMS-87-3-343, 2006.

Nakanishi, M. and Niino, H.: An improved Mellor-Yamada level-3 model: Its numerical stability and application to a regional prediction of advection fog, Bound.-Layer Meteorol., 119, 397–407, https://doi.org/10.1007/s10546-005-9030-8, 2006.

Pitt, J. R., Lopez-Coto, I., Hajny, K. D., Tomlin, J., Kaeser, R., Jayarathne, T., Stirm, B. H., Floerchinger, C. R., Loughner, C. P., Gately, C. K., Hutyra, L. R., Gurney, K. R., Roest, G. S., Liang, J., Gourdji, S., Karion, A., Whetstone, J. R., and Shepson, P. B.: New York City greenhouse gas emissions estimated with inverse modeling of aircraft measurements, Elementa: Science of the Anthropocene, 10, https://doi.org/10.1525/elementa.2021.00082, 00082, 2022.

Powers, J. G., Klemp, J. B., Skamarock, W. C., Davis, C. A., Dudhia, J., Gill, D. O., Coen, J. L., Gochis, D. J., Ahmadov, R., Peckham, S. E., Grell, G. A., Michalakes, J., Trahan, S., Benjamin, S. G., Alexander, C. R., Dimego, G. J., Wang, W., Schwartz, C. S., Romine, G. S., Liu, Z., Snyder, C., Chen, F., Barlage, M. J., Yu, W., and Duda, M. G.: THE WEATHER RESEARCH AND FORECASTING MODEL Overview, System Efforts, and Future Directions, Bull. Amer. Meteorol. Soc., 98, 1717–1737, https://doi.org/10.1175/BAMS-D-15-00308.1, 2017.

Ren, X., Salmon, O. E., Hansford, J. R., Ahn, D., Hall, D., Benish, S. E., Stratton, P. R., He, H., Sahu, S., Grimes, C., Heimburger, A. M. F., Martin, C. R., Cohen, M. D., Stunder, B., Salawitch, R. J., Ehrman, S. H., Shepson, P. B., and Dickerson, R. R.: Methane Emissions From the Baltimore-Washington Area Based on Airborne Observation: Comparison to Emissions Inventories, J. of Geophys. Res., 123, 8869–8882, https://doi.org/10.1029/2018JD028851, 2018.

Ryoo, J.-M., Iraci, L. T., Tanaka, T., Marrero, J. E., Yates, E. L., Fung, I., Michalak, A. M., Tadić, J., Gore, W., Bui, T. P., Dean-Day, J. M., and Chang, C. S.: Quantification of CO_2 and CH_4 emissions over Sacramento, California, based on divergence theorem using aircraft measurements, Atmos Meas Tech., 12, 2949–2966, https://doi.org/10.5194/amt-12-2949-2019, 2019.

Saunier, O., Mathieu, A., Didier, D., Tombette, M., Quelo, D., Winiarek, V., and Bocquet, M.: An inverse modeling method to assess the source term of the Fukushima Nuclear Power Plant accident using gamma dose rate observations, Atmos. Chem. Phys., 13, 11403–11421, https://doi.org/10.5194/acp-13-11403-2013, 2013.

Stein, A. F., Draxler, R. R., Rolph, G. D., Stunder, B. J. B., Cohen, M. D., and Ngan, F.: NOAA's HYSPLIT atmospheric transport and dispersion modeling system, Bull. Amer. Meteorol. Soc., 96, 2059–2077, https://doi.org/10.1175/BAMS-D-14-00110.1, 2015.

Stohl, A., Seibert, P., Wotawa, G., Arnold, D., Burkhart, J. F., Eckhardt, S., Tapia, C., Vargas, A., and Yasunari, T. J.: Xenon-133 and caesium-137 releases into the atmosphere from the Fukushima Dai-ichi nuclear power plant: determination of the source term, atmospheric dispersion, and deposition, Atmos. Chem. Phys., 12, 2313–2343, https://doi.org/10.5194/acp-12-2313-2012, 2012.

United States Environmental Protection Agency (U.S. EPA): Field Audit Checklist Tool (FACT), https://www.epa.gov/airmarkets/field-audit-checklist-tool-fact, version 1.6.0.3, 2022.

Walmsley, J. L. and Wesely, M. L.: Modification of coded parametrizations of surface resistances to gaseous dry deposition, Atmos. Environ., 30, 1181–1188, https://doi.org/10.1016/1352-2310(95)00403-3, 1996.

Wesely, M. L.: Parameterization of surface resistances to gaseous dry deposition in regional-scale numerical models, Atmos. Environ., 23, 1293–1304, https://doi.org/10.1016/0004-6981(89)90153-4, 1989.

Winiarek, V., Bocquet, M., Saunier, O., and Mathieu, A.: Estimation of errors in the inverse modeling of accidental release of atmospheric pollutant: Application to the reconstruction of the cesium-137 and iodine-131 source terms from the Fukushima Daiichi power plant, J. Geophys. Res. - Atmos., 117, D05 122, https://doi.org/10.1029/2011JD016932, 2012.

Winiarek, V., Bocquet, M., Duhanyan, N., Roustan, Y., Saunier, O., and Mathieu, A.: Estimation of the caesium-137 source term from the Fukushima Daiichi nuclear power plant using a consistent joint assimilation of air concentration and deposition observations, Atmos. Environ., 82, 268–279, https://doi.org/10.1016/j.atmosenv.2013.10.017, 2014.

665